

INVESTIGATION OF SELF-ORGANISATION IN THE BENARD EXPERIMENT
BASED ON MICRO-SCALE SIMULATION

by

Emre Kaya

B.S., Mechanical Engineering, Boğaziçi University, 2012

Submitted to the Institute for Graduate Studies in
Science and Engineering in partial fulfillment of
the requirements for the degree of
Master of Science

Graduate Program in Systems and Control Engineering
Boğaziçi University

2017

ACKNOWLEDGEMENTS

This thesis is an outcome of four years long period. Many people have been in and out of my life during this time, many things have changed, so I apologise for missing to mention any-who who has contributed to this work.

The whole process was similar to learning how to swim. From time to time, I felt like I was left alone in the middle of the sea. I struggled a lot, but at last, hopefully, I am enjoying being in harmony with my environment.

This thesis would not be possible without necessary conditions, namely Dynamic Systems Lab at Boğaziçi University and my dear supervisor, Yağmur Denizhan. She was brave enough to set off investigating such an interdisciplinary subject with me and I can not imagine doing this work with someone else. I would like to thank her for being there when I was hopeless, for never stopping to dedicate at least an hour of her schedule every week and all these ideas she inspired me with. Beside all the knowledge about dynamic systems, she has also taught me a great deal about thinking critically and communicating my work to the audience, and pushed me towards thinking about life and science.

I would like to thank warmly to my jury members, Leyla Gören and Teoman Turgut for their interest in my work and their evaluation. They provided me positive motivation in both of my presentations.

Many thanks to Koray who was always there in the quite long course of this process. I know that I was very unbearable most of the time, so thank you for tolerating me when I could not tolerate myself.

And finally, I would like to express my gratitude to my family. Although I think they never understood what I did and complained about the length of my studies, they were always there when I needed.

ABSTRACT

INVESTIGATION OF SELF-ORGANISATION IN THE BÉNARD EXPERIMENT BASED ON MICRO-SCALE SIMULATION

Self-organisation is the phenomenon where in a dynamic system made of autonomous, yet interacting components a global macro-scale regularity observable by an outside observer spontaneously emerges. Rayleigh-Bénard Convection is one of the most common examples of this phenomenon.

In this thesis, the Bénard experiment, which involves the self-organisation of convection cells, has been simulated at micro-scale, i.e. at molecular level, in order to investigate the dynamics underlying this self-organisation phenomenon at its most fundamental level. Molecular dynamics simulations of the proposed 2D micro-scale model have been conducted under different external conditions to observe the dynamic behaviour range of the system. An image processing algorithm based on curl of the velocity field has been developed to automatically detect the presence or absence of convection cells and thus the type of the dynamic regime at hand.

The 2D micro-scale model developed in this thesis sheds light on how the dynamic regime depends on external conditions and provides an answer to the original question of this study whether the emergence of macro-scale order can be detected from the micro-scale perspective of a single particle.

ÖZET

BENARD DENEYİNDE ÖZ-ÖRGÜTLENMENİN MİKRO-ÖLÇEKLİ BENZETİMLE İNCELENMESİ

Öz-örgütlenme, birbiriyle etkileşim halindeki otonom komponentlerden oluşan dinamik bir sistemde dışsal bir gözlemci tarafından gözlemlenebilir makro-ölçekte düzenli bir yapının kendiliğinden ortaya çıkması olgusudur. Rayleigh-Bénard Konveksiyonu bu olgunun en bilinen örneklerinden biridir.

Bu tezde, konveksiyon hücrelerinin öz-örgütlenmesine dayanan Bénard deneyi mikro-ölçekte, yani moleküler seviyede, simüle edilerek bu öz-örgütlenme olgusunun altında yatan dinamik en temel düzeyde incelenmiştir. Önerilen iki boyutlu mikro-ölçekli model üzerinde çeşitli dış koşullar altında moleküler dinamik benzetimleri gerçekleştirilerek sistemin dinamik davranış yelpazesi araştırılmıştır. Konveksiyon hücrelerinin var olup olmadığı ve böylece dinamik rejimi saptamak için hız alanının rotasyoneline dayanan bir görüntü işleme algoritması geliştirilmiştir.

Bu tezde geliştirilen 2 boyutlu mikro-ölçekli model, dinamik rejimin dış koşullardan nasıl etkilendiğine ışık tutmakta ve bu çalışmanın orijinal sorusuna, yani makro-ölçekte bir düzenin oluşumunun tek bir parçacığın mikro-ölçekli perspektifinden bakılarak tespit edilip edilemeyeceğine bir cevap vermektedir.

TABLE OF CONTENTS

ACKNOWLEDGEMENTS	iii
ABSTRACT	v
ÖZET	vi
LIST OF FIGURES	ix
LIST OF TABLES	xi
LIST OF SYMBOLS	xii
LIST OF ACRONYMS/ABBREVIATIONS	xiv
1. INTRODUCTION	1
1.1. Self-Organisation and Emergence	1
1.2. Bénard Experiment	2
1.3. Methods Used In The Study of Rayleigh-Bénard Convection	3
1.4. Thermodynamic Concepts: Equilibrium vs Non-equilibrium	4
2. PROBLEM STATEMENT AND SCOPE OF THE THESIS	6
3. MODELS AND SIMULATIONS IN THE LITERATURE	7
3.1. Macro-scale Models	7
3.2. Micro-scale Models	8
4. METHODOLOGY	10
4.1. Molecular-Dynamics-Based Simulation	10
4.1.1. Defining the Fundamental Building Blocks	12
4.1.2. Interactions between Particles	12
4.1.3. Dimensionless Units	15
4.1.4. Choice of the Initial Conditions	17
4.1.5. Modelling the Boundaries	17
4.1.6. Thermostatting and Heat Exchange	19
4.1.7. Numerical Integration and Simulation Duration	21
4.2. Analysis of the Simulation Results	21
4.2.1. Ensemble Analysis	21
4.2.1.1. Coarse Graining and Computation of the Flow Field	21
4.2.1.2. Automatic Detection of the Dynamic Regime	23

4.2.2.	History Analysis of a Single Particle	30
4.2.2.1.	Computation of the Flow Field and Automatic Detec- tion of Convection Cells	31
4.2.2.2.	Automatic Detection of the Dynamic Regime from Force History	31
5.	SIMULATION RESULTS AND THEIR ANALYSIS	32
5.1.	Ensemble Analysis	32
5.1.1.	Construction of the Flow Field	32
5.1.2.	Automatic Detection of Convection Cells	37
5.2.	History Analysis of a Single Particle	37
5.2.1.	Construction of the Flow Field	37
5.2.2.	Automatic Detection of Convection Cells	40
5.2.3.	Can the Macro-Scale Dynamic Regime be Detected from the Particle Perspective ?	45
6.	CONCLUSION	49
	REFERENCES	51
	APPENDIX A: NUMERICAL INTEGRATION ALGORITHM	54

LIST OF FIGURES

Figure 1.1.	Top view of the convection cells, from Bénard’s original experiment [1].	3
Figure 4.1.	Dimensionless Lennard-Jones 6-12 potential and force versus dimensionless interatomic distance.	14
Figure 4.2.	Dimensionless Lennard-Jones 6-12 potential and force versus dimensionless interatomic distance, with cutoff at 1.122.	15
Figure 4.3.	Heat layers of the simulation domain.	20
Figure 4.4.	The process of spatio-temporal coarse graining.	22
Figure 4.5.	Streamline and vorticity contour correspondence for a given velocity field.	25
Figure 4.6.	Steps of automatic detection algorithm described on a vector field obtained from a simulation with AR=0.9.	26
Figure 4.7.	Allowed region for centres for a container with size 1×1 . Numbers on the axes represent the % distances from the boundaries.	27
Figure 4.8.	Velocity and vorticity fields of an ideal vortex.	28
Figure 4.9.	Dendrogram representing the clustering of centres, cut from Euclidean distance of 30 (vertical blue line).	30
Figure 5.1.	Flow Field for AR=0.9.	33

Figure 5.2.	Flow Field for AR=1.4.	34
Figure 5.3.	Flow Field for AR=1.8.	35
Figure 5.4.	Steps performed in the automatic detection of a single convection cell.	38
Figure 5.5.	Location of the centre of single convection cell.	39
Figure 5.6.	(a) Centroids and (b) their clustering for a velocity field with 2 convection cells.	39
Figure 5.7.	(a) Centroids and (b) their clustering for a velocity field with 3 convection cells.	40
Figure 5.8.	Velocity and position history of a single particle at convection regime ($\Delta T = 10$).	41
Figure 5.9.	Velocity and position history of a single particle at convection regime ($\Delta T = 4$).	42
Figure 5.10.	Automatic detection algorithm applied on single particle history, case of single vortex.	43
Figure 5.11.	Automatic detection algorithm applied on single particle history, case of three vortices.	44
Figure 5.12.	Force history and its FFT for a particle in convection regime.	47
Figure 5.13.	Force history and its FFT for a particle in conduction regime under three different temperature gradients.	48

LIST OF TABLES

Table 4.1.	Lennard-Jones parameter values for argon.	13
Table 4.2.	Physical variables of the simulation and their dimensionless counterparts [2].	16

LIST OF SYMBOLS

d	Height of the container
E	Energy
\mathbf{F}	External force acting on particle
\mathbf{g}	Gravitational acceleration
k_b	Boltzmann constant
m	Mass of a particle
n	Width of coarse graining time window
n_τ	Width of root-mean-square time window
N	Number of particles
\mathbf{r}_{ij}	Displacement between particle i and particle j
r_c	Cut-off distance for LJ potential
Ra	Rayleigh number
t	Time
T	Temperature
\mathbf{v}	Velocity of particle
V_{cell}	Grid cell size
\mathbf{x}	Position of particle
α	Thermal conductivity
Δt	Time step
ΔT	Temperature difference
ϵ	Depth of energy for interatomic LJ potential
ϵ_{wall}	Depth of energy for wall-particle LJ potential
ζ	Dynamic regime index
κ	Thermal conductivity
λ_v	Velocity rescaling factor
ν	Kinematic viscosity
ρ	Number density

σ	Equilibrium distance for interatomic LJ potential
σ_{wall}	Equilibrium distance for wall-particle LJ potential
σ_{filter}	Standard deviation of Gaussian image filter
Φ_{ij}	Interatomic potential between particles i and j
ω	Vorticity
∇	Del operator

LIST OF ACRONYMS/ABBREVIATIONS

2D	Two Dimensional
3D	Three Dimensional
AR	Aspect Ratio
FFT	Fast Fourier Transform
KE	Kinetic Energy
LJ	Lennard-Jones 6-12
MD	Molecular Dynamics
PE	Potential Energy
ODE	Ordinary Differential Equation
RBC	Rayleigh-Bénard Convection
SI	International System of Units

1. INTRODUCTION

1.1. Self-Organisation and Emergence

Self-organisation is the phenomenon where a dynamic system made of autonomous, individual agents appears to show evidence of global order and pattern to an outside observer. As the word “self” suggests, the organisation occurs only due to local interactions between the agents without any external regulatory effect [3].

Haken defines a self-organising system as a system acquiring a spatial, temporal or functional structure without specific interference from the outside. He further explains that the term “specific” is used to emphasize that the appearing structure is not imposed on the system but that the system is acted upon from the outside in a nonspecific fashion [4].

As defined by Camazine, “Self-organisation is a process in which pattern at the global level of a system emerges solely from numerous interactions among the lower-level components of the system. Moreover, the rules specifying interactions among the system’s components are executed using only local information, without reference to the global pattern” [5].

All these definitions capture three important aspects of the phenomenon of self-organisation: First, it is assumed that the system has many interacting components and advances from a less organised state to a more organised state dynamically over some time while exchanging energy, matter, and/or information with the environment. Second, this organisation is manifested via global coordination, and the global behaviour of the system is a result of the interactions among the agents. Finally, the components, whose properties and behaviours are defined prior to the organisation itself, have only local information and do not have knowledge of the global state of the system therefore, self-organisation process involves some local information transfer [6].

There exist many examples of self-organisation in a wide range of physical, biological and social systems both in popular and academic literature. Phase transitions, lasers, flocking of birds, consensus achievement of group of people are among the most cited examples.

Emergence of order at global scale is a common property among all these examples. Due to controversial and somewhat questionable nature of the term “order”, the discussions about what is called “ordered” and “unordered” will be left beyond the investigation of this thesis. Here, the concept of order for a system will be related to the existence of coherent structures that can be spotted by an observer existing at a higher scale than that of agents the system.

Another important example of self-organisation, which constitutes the subject of investigation in this thesis, is Bénard’s experiment.

1.2. Bénard Experiment

In 1901, Henri Bénard performed an experiment in order to understand how a fluid behaves under different environmental conditions. In his experiment, he filled a rectangular prism shaped container with a high aspect (width to height) ratio by a viscous fluid. Then, he supplied uniform heat from the bottom plate of the container while insulating the lateral ends but leaving the upper plate open to the atmosphere i.e he created (quasi-)one dimensional heat flux in the opposite direction of gravity. As he further increased the heat flux, after a certain threshold, he observed rotating rolls in the fluid which moved from the lower plate to the upper one and then back.

This experiment suggests that a fluid in a container with a certain geometry and fluid properties (such as viscosity, density etc.) shows different qualitative behaviours depending on the degree of heat flux it is submitted to. In the following years of this experiment, theoretical explanations of this phenomenon has been given by Lord Rayleigh [7]. Due to contributions of these two scientists, today, the phenomenon is known as Rayleigh-Bénard Convection (RBC).

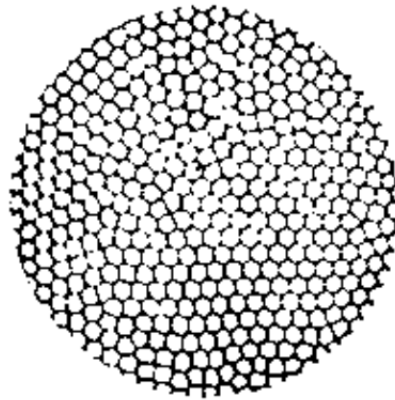


Figure 1.1. Top view of the convection cells, from Bénard's original experiment [1].

From a dynamical systems point of view, such a system manifests a bifurcating behaviour which gives birth to persisting stationary coherent structures called Bénard cells (Figure 1.1) sensitive to changes in heat flux. The formation of Bénard cells is an emergent phenomenon, appearing automatically, imposed by no other external agent on the system.

1.3. Methods Used In The Study of Rayleigh-Bénard Convection

So far, RBC have been studied in different resolutions and by different means depending on the purpose of the study:

- **Experimental Approach:** Explained above, as in the study of Henri Bénard.
- **Macro-scale Model:** Macro-scale studies based on continuum assumption are performed using the well-known and well-developed (partial differential) equations of fluid mechanics and heat transfer. By applying a perturbation to the equations of natural convection the conditions for the onset of instability can be calculated analytically.
- **Macro-scale Simulations:** The partial differential equations that constitute the macro-scale analytical model can be solved by various numerical methods of com-

putational fluid dynamics.

- **Micro-scale Model and Simulations:** At the molecular level, the fluid is defined as a collection of atoms/molecules moving and interacting with each other. Information regarding the macro-variables (such as density, temperature etc.) can be obtained by taking spatial and temporal averages on the kinetic and potential energies of these atoms/molecules. This approach gives the maximum information about the micro-scale phenomena, but is the computationally costly method. This approach is the one adopted in this thesis.

1.4. Thermodynamic Concepts: Equilibrium vs Non-equilibrium

At this point, it is necessary to give some thermodynamic definitions that will be used throughout the thesis.

From a thermodynamic point of view, pattern forming systems, such as RBC, are systems that are maintained out of equilibrium [8]. The distinction between an equilibrium system and a nonequilibrium system is made according to the existence of transport phenomena within the system.

A system is in equilibrium if there are no gradients of temperature, velocity or density within the system, so that these variables are, on average, constant both in space and time. Conversely, a system is in nonequilibrium when the gradients of the above variables are present and these variables create thermodynamic fluxes within the system.

There exists three kinds of systems in terms of the relation with their surroundings: *isolated systems* do not interact with their environments, *closed systems* can exchange energy with their environments and *open systems* can exchange both energy and matter with their environments.

By definition, Bénard's system is a nonequilibrium one that exchanges energy with its environment, thus constitutes an open system. To create such a system, one

must induce momentum or energy flow into simulation and drive the system out-of-equilibrium. [9]

2. PROBLEM STATEMENT AND SCOPE OF THE THESIS

In his article, Rapaport says: “While considerable progress has been made in understanding of this (Bénard) experiment by means of stability analysis and model calculations that address simplified versions of the hydrodynamic equations governing the system, a full theoretical understanding of the symmetry breaking and mode selection mechanisms at work in this comparatively simple dynamical process has yet to be achieved” [10].

Setting off from such an observation, the main purpose of this work is to investigate and understand the process of self-organisation in the RBC by setting an analogy via molecular dynamics (MD).

Thus, the task in this study is twofold: (i) to obtain an MD simulation that is able to qualitatively mimic Bénard’s experiment, (ii) to study the dynamics of the process that will hopefully reveal the mechanics of symmetry breaking and mode selection.

The organisation of the thesis is as follows: chapter 3 is dedicated to an overview of the literature that involves the studies of RBC via MD. In chapter 4, the procedural details of MD simulations and analysis methods are presented. In chapter 5, the outcomes of these simulations are presented and finally in chapter 6, these results are interpreted.

3. MODELS AND SIMULATIONS IN THE LITERATURE

3.1. Macro-scale Models

After Bénard's experiment, Lord Rayleigh provided the stability analysis for the phenomenon using hydrodynamic equations, in 1916. These include solutions of incompressible Navier-Stokes and energy equations under appropriate boundary and initial conditions. For simplifying the solutions, an approximation called Boussinesq approximation is applied, which states that the density is a function of the temperature only [1]. Full derivation of this analysis can be found at [11]. Rayleigh's analysis suggests an order parameter noted by his name, Rayleigh number (Ra), the value of which determines the degree of instability within the system. Ra is defined as:

$$Ra = \frac{g\alpha\Delta T d^3}{\nu\kappa} \quad (3.1)$$

When $Ra \approx 1708$, first instability occurs and the mode of heat transport shifts from conduction to convection, hence convection cells appear. Physically, this regime shift is explained by competing forces of buoyancy, gravity, thermal and viscous dissipation within the fluid. At low values of Ra , heat from lower to upper plate is transferred via conduction and there is no bulk motion within the fluid. In this case, vertical temperature and density profiles of the fluid are linear. As Ra is increased, density gradient within the fluid becomes steeper and steeper: hot parcels of fluid become lighter, which try to move towards the upper plate due to buoyancy forces and in turn, cold parcels which are denser try to move towards lower plate due to gravity. As Ra reaches its critical value, these forces overcome thermal and viscous dissipation forces and the convection sets in [1].

Bénard's was the first experiment to show this instability, but was not the last. In the over past 100 years following this preliminary work, many replications and variants of this experiment are performed.

3.2. Micro-scale Models

Molecular dynamics simulations started to appear in the scientific literature after the invention of the necessary prerequisite, namely the digital computer, in the 1950s.

First work involving molecular dynamics of Rayleigh-Bénard convection [12] appeared much later, in 1987, perhaps due to the relatively high computer power required to run simulations with high number (at least order of 1000) of molecules. This first work performed by Mareschal et al., involved 5040 hard disks in a box with aspect ratio 2.83, and a number density of 0.2. Atoms were placed randomly inside the simulation domain and their velocity were chosen from equilibrium distributions at the local temperature from a linear temperature between plates. Boundaries of the simulation domain acted as walls: lateral walls reflected the atoms while at the heat walls, tangential component of the velocity was kept and the normal component was resampled from local temperature. To drive the system out of equilibrium, hot and cold wall temperatures were adjusted to 10 and 1 respectively and a gravitational acceleration of 0.09 was applied in the inverse direction of the temperature gradient. As a result, 3 vortices were observed by coarse graining the system within 20x50 cells, but these vortices were found not to be lasting for very long time.

The next work on MD simulation of RBC was by Rapaport in 1988 [10], which was still in 2D and was performed using hard disks in a box with aspect ratio 4 but involved more disks (14160) and a higher number density (0.4). Differently from previous work, lateral walls of the simulation domain were periodic in order to eliminate side wall effects. By applying a higher temperature gradient ($\Delta T = 16$), four stable rolls were observed within the coarse grained cells. Main result of this work was the requirement of high number density for the appearance of stable rolls.

The work of Rapaport in 1992 [13] was still performed using hard disks, but this time, the number of disks was quadrupled (57600 disks) and also octupled (115600 disks) while keeping the number density as in the previous case (0.4). Performed in a square box, with hot wall temperature of 16 and rough walls, this simulation permitted

to two vortices. These two vortices were found to be coherent and their centres were found to be oscillating.

First documented work involving soft disks dated to 2006 [14], which was still by Rapaport. This work documented a simulation in 3D with width to length ratio almost 1 and aspect ratio of 14. Lateral walls of the simulation domain were periodic and thermal walls consisted of a layer of fixed atoms. Velocity of the atoms were rescaled to the velocity close to desired temperature values close to these walls. Regarding initial conditions, atoms were placed on a regular grid with random velocities corresponding to the uniform temperature gradient. Again, in order to obtain the macroscopic field variables, coarse graining was used with averages in time as well. Two types of structures were observed: first being the hexagonal array of cells and the other, linear array of rolls.

Last work involving MD simulation of RBC [15] investigated, for the first time, the transient evolution of the Bénard cells rather than the steady-state cells that appear at the end of the simulation. The simulation consisted of 5041 particles in 2D, between which Weeks-Chandler-Andersen potential was used. Number density was kept at 0.4, and hot wall temperature was adjusted to 12.2. Thermal walls were assumed to be repulsive. Coarse graining analysis included ensemble averages instead of time averages: 480 identical systems were run with different initial conditions to gather the data used in the generation of the velocity field.

4. METHODOLOGY

The main purpose of this thesis is to develop a micro-scale model for the Bénard experiment that is capable of exhibiting the macro-scale behaviour of self-organisation.

As a modelling principle the model is kept as simple as possible but complex enough to allow the emergence of Bénard cells. It is not intended to stick to the physical realm and deduce physical properties of such a system by the methods of statistical mechanics. Rather than that the aim is to investigate the phenomenon of self-organisation itself in a qualitative manner.

4.1. Molecular-Dynamics-Based Simulation

Methods so far used in the study of Rayleigh-Bénard convection include analytical solutions to continuum mechanics equations, numerical simulations of these equations, experimentation and simulation using molecular dynamics [10, 12, 13, 16, 17]. Among these methods, only molecular dynamics permits a view into the micro universe of the tiniest constituents of the substance under study (such as molecular trajectories) and provides information about the mechanisms underlying the emergence of macro-scale structures, thus molecular dynamics has been adopted as the modelling approach in this study.

Very roughly, molecular dynamics is the study of behaviour of substances based on their atomistic description that starts from an initial state and keeps track of the forces, velocities and positions as the system evolves over time. Once these variables are computed, one can obtain the thermodynamic (macroscopic) properties of the system (such as pressure and temperature, or transport properties as viscosity and thermal conductivity) by means of statistical mechanics. [18]

With the simplest approach, substances can be thought to be made of identical particles that can be hypothetically accepted as atoms or molecules. Classical MD

states that these particles should obey Newton's second law: then, for a single particle with index i within this substance, equation of motion is simply given as:

$$\Sigma \mathbf{F}_i = m \ddot{\mathbf{x}}_i$$

where \mathbf{F}_i designates the sum of all external forces acting on the i th particle, and $\ddot{\mathbf{x}}_i$ its acceleration.

Using the position, $\mathbf{x} = \left[\mathbf{x}_1 \ \dots \ \mathbf{x}_i \ \mathbf{x}_{i+1} \ \dots \ \mathbf{x}_N \right]_{2N \times 1}^T$ and the velocity, $\mathbf{v} = \left[\mathbf{v}_1 \ \dots \ \mathbf{v}_i \ \mathbf{v}_{i+1} \ \dots \ \mathbf{v}_N \right]_{2N \times 1}^T$ as state vectors, , the dynamics of the i th particle can be written as a system of 2 first order vector differential equations:

$$\begin{aligned} \dot{\mathbf{x}}_i &= \mathbf{v}_i \\ \dot{\mathbf{v}}_i &= \frac{\Sigma \mathbf{F}_i}{m} \quad \forall i = 1, \dots, N \end{aligned} \quad (4.1)$$

Then, for a substance composed of N particles, equations of motion consist of $2N$ coupled differential vector equations, leading to $4N$ equations in two-dimensional Cartesian coordinates.

Before solving the equations 4.1 $\forall i = 1, \dots, N$, the following modelling and simulation properties need to be determined:

- Interatomic potential between particles
- Initial conditions of the simulation
- Boundary conditions which define the boundaries of the simulation domain and determine how the particles interact with the boundaries
- Numerical algorithm to be employed for solving the ordinary differential equations (ODEs) in equations 4.1.

4.1.1. Defining the Fundamental Building Blocks

Metaphorically, creating a box filled with particles ¹ can be considered as creating a group of bouncing balls within a container. Certainly, this model is far from reflecting the actual complex behaviour of the molecules of the fluid in Bénard experiment, but has the advantage of computational simplicity. [2].

It is known that some noble gases can be modelled fairly accurately as a simple fluid [19]. One of the simplest and the most preferred of such substances is argon. Argon is a mono-atomic noble gas having few degrees of freedom: it has only 2 translational degrees of freedom in two dimensional Cartesian coordinates, making calculations simpler. Also, referring again to previous studies [14] and [15], it has been shown that the RBC phenomenon manifests itself even with that simple fluid. Thus argon is selected as the particle employed in the simulations.

4.1.2. Interactions between Particles

There exist two main approaches to modelling how particles interact and exchange their momenta:

- The first one does not account for any potential between particles and assumes the velocity to remain constant until a collision occurs. Here, the momentum exchange is modelled as an elastic collision. This type of particles are referred to as “hard disks” or “hard balls”.²
- Alternatively, particles may be modelled as interacting with each other via a specified interatomic potential that is a function of the interatomic distance. This second type of particles are called “soft disks” or “soft balls” depending on dimensionality of the simulation.

¹From this point on, the fluid atoms/molecules will be referred to as particles.

²The terms “hard balls” (used for 3D simulation) and “hard disks” (used for 2D simulation) depend on the dimensionality of the simulation.

In soft disk simulations, any pair of particles can either repel or attract each other [2]. In that manner, the interatomic potential behaves as a (non-linear) spring that conserves the total mechanical energy.

In the literature, there exist different empirically derived interatomic potentials depending on the complexity and type of the particle to be studied. One of the commonly implemented potentials, the Lennard-Jones 6-12 (LJ) potential between i th and j th particles is defined as:

$$\Phi_{ij} = 4\epsilon\left[\left(\frac{\sigma}{|\mathbf{r}_{ij}|}\right)^{12} - \left(\frac{\sigma}{|\mathbf{r}_{ij}|}\right)^6\right] \quad (4.2)$$

The values of parameters σ and ϵ are unique to any type of particle selected for the simulation. σ indicates the interatomic distance where the interaction between particles is zero and ϵ designates the minimum value of the interatomic potential. The values of these parameters for argon is given in 4.1.

Table 4.1. Lennard-Jones parameter values for argon.

Parameter	Value in SI
σ	$3.4 \cdot 10^{-10}$ Meters
ϵ	$1.65 \cdot 10^{-21}$ Joules
ϵ/k_b	120 Kelvins

The interatomic force can then be expressed as the gradient of the potential:

$$\mathbf{F}_{ij} = \nabla\Phi_{ij} \quad (4.3)$$

Plotting equations 4.2 and 4.3 versus dimensionless distance (r_{ij}/σ), which is given in Figure 4.1, two main interpretations can be made regarding their form:

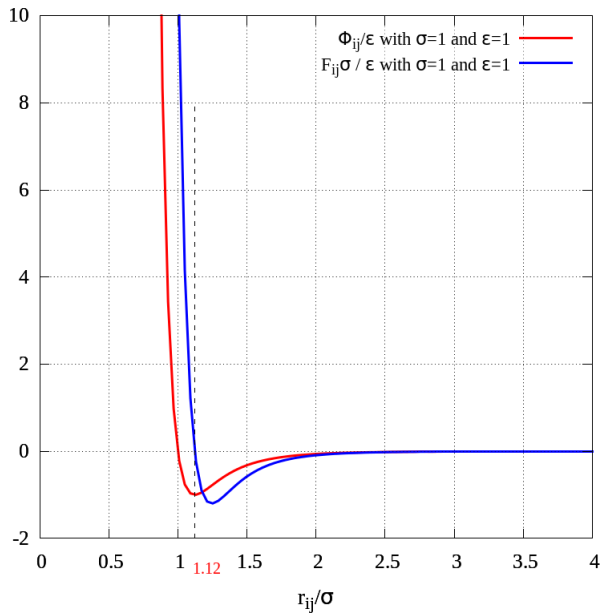


Figure 4.1. Dimensionless Lennard-Jones 6-12 potential and force versus dimensionless interatomic distance.

- At short distances, there exists a strong repulsion (as $r_{ij} \rightarrow 0$, $\Phi_{ij} \rightarrow \infty$).
- At relatively medium and long distances, there exists a weak attraction (as $r_{ij} \rightarrow \infty$, $\Phi_{ij} \rightarrow 0$).

Since force calculations constitute the part of MD simulations that demands the largest portion of computational power [2], it is a common practice to use some simplifying assumptions about the potential such that less computational power is spent at this step and simulations take less time. such as potential is truncating the potential at a certain distance. For that purpose, the potential is truncated for distances above $r_c = 1.122$, which belongs to the minimum of the potential. New potential is given in Figure 4.2.

Noticing again the quick increase of the potential towards low distances, which may cause stability problems for the simulation, value of ϵ is chosen as 0.5ϵ instead of ϵ although this choice did not considerably decrease the steepness of the potential.

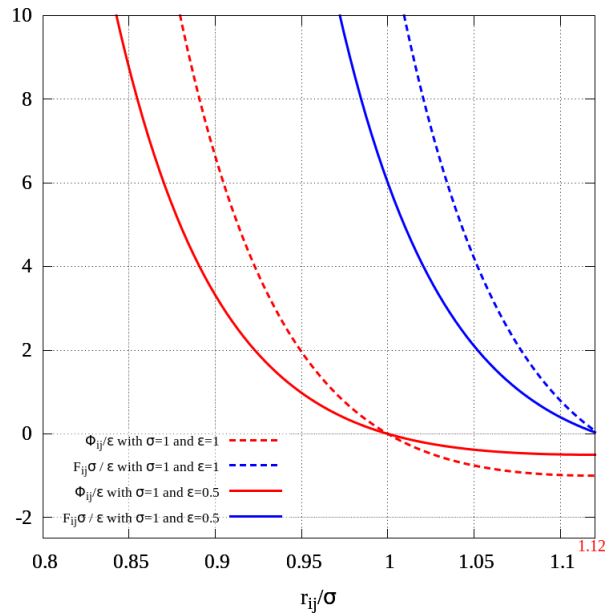


Figure 4.2. Dimensionless Lennard-Jones 6-12 potential and force versus dimensionless interatomic distance, with cutoff at 1.122.

The other external force acting on the particles, force due to gravitational acceleration, g , is selected to be 0.15.

4.1.3. Dimensionless Units

In science and engineering, physical variables are defined by their dimension, to which a list of units may be assigned: a dimension is a measure that defines a characteristic of a variable and a unit is a way of assigning a number to that dimension. For example, length is a dimension that is measured in units such as meters or feet. A physical variable can be scaled with a parameter that has the same dimension to obtain a dimensionless variable [20].

Dimensionless variables have the following advantages over dimensional variables:

- In MD, one deals with atoms, so the scale and units are typically very small, 10 to 20 orders of magnitude smaller than SI units. Appropriate nondimensionalisation

of these units allows one to work with numbers close to unity rather than very small numbers. [2]

- Numerical errors can be reduced.
- The parameters in the equation of motion are absorbed into nondimensional parameters. Those simplified equations have less parameters [2]
- Dimensionless equations provide scaling and universality: Irrespective of properties of the simulated solid/fluid type, one can solve the dimensionless equations of motion and then obtain the values of the desired fluid using its non-dimensionalizing parameters. [2]

In MD, it is convenient to use 3 scaling parameters: σ , ϵ and m in order to replace length, energy and mass dimensions. The rest of the variables can be nondimensionalised using multiplicative or divisive combinations of these three scaling parameters. A list, together with variables and their dimensionless counterparts is given in table 4.2.

Table 4.2. Physical variables of the simulation and their dimensionless counterparts [2].

Physical Variable	Non-dimensional Form
Displacement, r	r/σ
Energy, E	E/ϵ
Time, t	$t/(\sigma/\sqrt{\epsilon/m})$
Velocity, v	$v/(\sqrt{\epsilon/m})$
Force, F	$F/(\epsilon/\sigma)$
Temperature, T	$T/(\epsilon/k_b)$

These variables can be computed using LJ potential parameters given in table 4.1 and mass of argon atom, m which is $6.69 \cdot 10^{-26}$ kilograms.

4.1.4. Choice of the Initial Conditions

Although it is expected that the dynamics described by the ODEs in equation 4.1 will settle down to a steady-state dynamic behaviour and hence the initial conditions will be “forgotten”, it is important to start the simulation from a sufficiently realistic initial configuration to assure a fast enough convergence to the steady-state dynamics.

A possible practical choice is to place the particles initially on a regular lattice of a preferred type (such as square or triangle for 2D simulations; cube or hexagon for 3D simulations) with a lattice spacing that corresponds to the desired number density i.e. number of particles per area or volume. Initial velocities may be assigned randomly such that the vector sum of velocities add up to zero to avoid bulk motion, i.e. total momentum is zero and the variance of the magnitude of the velocity distribution gives the desired temperature. [2]

In this thesis, the particles have been initially placed on a square lattice with number density equal to 0.6. This choice provides an initial spacing of ≈ 1.3 between the particles, such that initially no interatomic forces are exerted on them.

Initial velocity assignment is made as follows: for each principal direction the respective velocity component is randomly assigned according to a Gaussian distribution with mean 0 and variance 1, assuming an equilibrium starting condition. As the simulation starts and proceeds, this artificially created initial conditions are forgotten through equilibration.

4.1.5. Modelling the Boundaries

Since the simulation takes place in a finite container, the simulation domain needs to be constrained by boundaries and it needs to be defined how particles interact with these boundaries [2].

Especially for relatively small container sizes, particle-boundary interactions constitute a relatively significant fraction of the total impact on the particles.

One method often used to avoid most of the problems associated with modelling the particle-boundary interactions is to assume periodic side walls. In such a setting, a particle leaving the container through one side wall re-enters it through the opposite one. Hence, in 2D, the simulation domain becomes equivalent to the surface of a cylinder. Even in this approach, however, one has to come up with an adequate model for the interactions with the top and bottom boundaries, if Bénard experiment is being simulated.

Alternatively, one can choose to model particle-boundary interactions for all sides. In this case, the common options are: (i) modelling the boundaries as an extra layer of atoms, (ii) introducing an interaction potential between the wall and the fluid particles (“smooth walls”) or (iii) updating the velocity of an atom instantaneously as it approaches the boundary (“hard walls”).

In this thesis, a particle-boundary potential is introduced at the boundaries. In terms of its form, this potential is the same as interatomic potential described in 4.1.2. For the purpose of obtaining a slightly stronger repulsive force so that the particles do not leave the simulation domain, values of σ_{wall} and ϵ_{wall} are adjusted to 1.1 and 2 respectively. The walls interact with particles only in normal direction, leaving the tangential velocity component constant.

Container height, d , (the dimension along the gravitational acceleration) is chosen to be 133.62 in dimensionless length. Width of the container is then computed using the aspect ratio (AR) of the container. Three different ARs are selected for the simulation: 0.9, 1.4 and 1.8. With the number density value of 0.6 and the given ARs, number of particles of simulations are calculated as 9579, 14935 and 19158 particles.

4.1.6. Thermostatting and Heat Exchange

In MD simulations, it may be necessary to keep a certain variable such as temperature or pressure constant within a certain region. Methods of fixing the temperature at a desired value are called as “thermostatting”.

The four different thermostats typically used in MD (velocity rescaling, Berendsen thermostat, Andersen thermostat, Nosé - Hoover thermostat) differ from each other in terms of how the desired temperature is reached i.e. convergence time and the type of the convergence behaviour.

Velocity rescaling is the simplest thermostat which consists of rescaling all the velocities within a region by a given factor after each integration step while keeping the positions fixed. For the i th particle, it is given as:

$$\mathbf{v}_i(t + \Delta t) = \lambda_v \mathbf{v}_i(t) \quad (4.4)$$

and the factor is calculated by:

$$\lambda_v = \sqrt{\frac{T_{des}(t + \Delta t)}{T(t)}} \quad (4.5)$$

where $T(t)$ is the the temperature at time t and $T_{des}(t + \Delta t)$ is the desired temperature at the next time step. and temperature is calculated using the total kinetic energy by

$$T = \frac{1}{2Nk_b} \sum_{i=1}^N m |\mathbf{v}_i|^2 \quad (4.6)$$

In this thesis, this thermostat is used for creating heat walls.

With the help of thermostatting, the system can be driven out-of-equilibrium. Using the analogy of Bénard experiment, two driving forces should be applied on

the system: gravity (acting in -y direction) and a thermal gradient directing in the opposite direction to the gravity. Gravitational acceleration is applied on every particle individually. Thermal gradient is created by tuning the temperature of the different regions of the container using thermostatting scheme explained above. In Bénard experiment, temperatures of two regions are controlled: the lower plate of the container, which is heated up and the upper plate of the container, which is open to atmosphere and thus is at ambient temperature.

A horizontal zone next to the lower boundary of the simulation domain is chosen for creating a hot wall, and another zone next to the upper boundary is chosen for creating a cold wall. The thickness of these regions are chosen to be 5% of the simulation domain. This value is chosen heuristically, expecting the zone to be thin enough not to disturb the dynamics, and thick enough to drive the system out-of-equilibrium. The regions of hot and cold walls, where thermostatting is applied will be collectively called as “heat layers”.

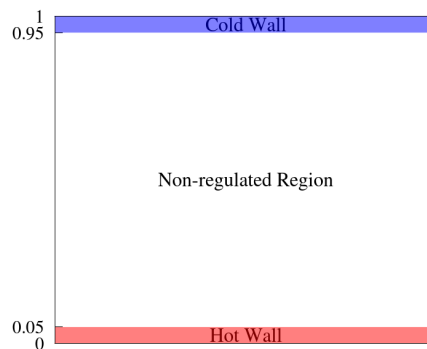


Figure 4.3. Heat layers of the simulation domain.

These thermostatted regions interact with the rest of the system (where the dynamics are of interest) via mass and energy exchange through a single side while the other sides are constrained to interact with the wall. The effect of thermostat is to scale the speed of the particles inside the thermostat region so that the temperature of these particles is kept at a desired value. The upper thermostat temperature has been set to 1, while the lower thermostat temperature is assigned different values from 2 to 11 depending on the temperature gradient applied to the system.

4.1.7. Numerical Integration and Simulation Duration

In this study, the velocity-Verlet (see appendix A for details) method with a time step of 0.005 has been used as an integration scheme (as advised by LAMMPS manual [21]). For very high temperature gradients, a time step of 0.004 is used for the sake of stability of the simulation.

Under these conditions, the simulation is run for a heuristically determined settling duration of 10000 steps in order to give the system enough time to reach steady-state and become independent of the somewhat arbitrarily assigned initial conditions. Then, the system is run for an additional of 5000000 time steps and the dynamics are investigated using the methods described in the following section.

4.2. Analysis of the Simulation Results

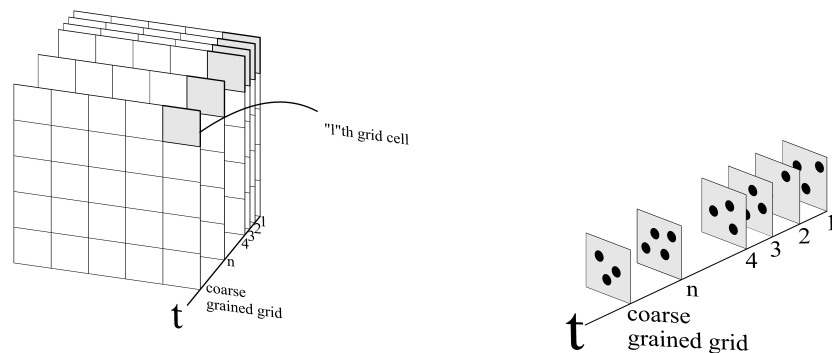
The simulation data can be analysed to identify the dynamic regime of the system under consideration. In this thesis, two different approaches have been employed for this purpose: (i) *ensemble analysis*, where, from positions and velocities of all particles at a given time after the system has reached steady-state, thermodynamic (macro-scale) variables of interest are computed, and (ii) *history analysis of a single particle*, where, from position, velocity and force history of a randomly selected particle, thermodynamic (macro-scale) variables of interest are computed.

4.2.1. Ensemble Analysis

4.2.1.1. Coarse Graining and Computation of the Flow Field. The process of coarse graining is performed by dividing the simulation domain into cells of desired size using a regular grid, and calculating the macro-scale variables in each cell from the distribution of variables within this cell. However, here coarse graining also contains a temporal dimension, because the macro variables for a grid cell are calculated using data about particles that visit this cell during a specific time window. The width of this window is chosen heuristically to sufficiently reduce the noise created by spatial discretisation.

In this sense, it is possible to call this process *spatio-temporal coarse graining* (Figure 4.4).

Also, the grid cell size, is a heuristically chosen parameter that is expected to provide a reasonable trade-off between smoothness of the flow and information conservation.



(a) Simulation domain is divided into grid cells.

(b) Particles within those cells are averaged both in space and time.

Figure 4.4. The process of spatio-temporal coarse graining.

The width of the temporal coarse graining time window, n , has been taken as 200 time steps. For the sake of reducing the computational burden, averages are updated every 20^{th} time step.

- **Density Field:** The density field is the spatial number density distribution obtained by coarse graining [9]. The number density, ρ_ℓ of the ℓ th grid cell is the total number of particles that have visited the ℓ th grid cell during a time window of n time steps averaged over grid cell size [19]

$$\rho_\ell = \left\langle \frac{N_\ell}{V_{cell}} \right\rangle_n \quad (4.7)$$

- **Velocity Field:** Similar to the density field, the velocity field is obtained by averaging velocity vectors of the particles within the ℓ th grid cell over n time steps. Representing the number of particles within the ℓ th cell at the i th time step with N_i , for ℓ th grid cell, the velocity vector can be expressed as:

$$\mathbf{v}_\ell = \frac{\sum_{i=1}^n \sum_{j=1}^{N_i} \mathbf{v}_i^j}{\sum_{i=1}^n N_i} \quad (4.8)$$

- **Temperature Field:** Within a coarse grained grid cell, the temperature is assumed to be uniform and it is calculated from the total kinetic energy-temperature equality, from equation 4.6 by using the velocities of the particles within this grid cell.

$$T_\ell = \frac{\sum_{i=1}^n \sum_{j=1}^{N_i} \frac{1}{2} m |\mathbf{v}_i^j|^2}{\sum_{i=1}^n N_i k_b} \quad (4.9)$$

The cold and hot layers shown in Figure 4.3 are excluded from the coarse graining process. The remaining part of the container is divided into 15 horizontal rows and as many columns as necessary to obtain almost square cells depending on the AR of the container. With such choice of cell size, the simulations in this thesis have involved approximately 42 particles per cell at a given time instance.

4.2.1.2. Automatic Detection of the Dynamic Regime. In macro-scale representations of RBC, instability analysis of equations of motion is the method used for identifying the dynamic regime. According to the values of the two dimensionless numbers, namely the Rayleigh and Reynolds numbers, computed mathematically, the dynamic regime can be predicted. On the other hand simulations of micro-scale models do not lend themselves to such an analysis, thus the regime should be identified by other means.

According to the well-established analytical thermodynamic model, when the temperature gradient between the top and the bottom is increased from zero, the first instability in RBC occurs as a regime shift, i.e. a change of the dominant mode of heat

transfer from conduction to convection. Emerging convection cells are a manifestation of this shift. Thus, the regime change can be assessed by detecting the existence of convection cells.

If the data are presented in an appropriate graphical form, the dynamic regime can be rather easily identified by a human observer via visual inspection. The simulation results obtained in this study have shown the convection cells can be most easily detected by visual inspection of the velocity fields, rather than of temperature or density fields. But, because of the subjectivity of the human inspector's decision, as well as the rapidly declining human performance as the number of detection tasks increases, it is desirable to develop an algorithm for the automatic detection of convection cells. The detection algorithm developed in this study tries to imitate the human observer's recognition process as far as possible.

In fluid dynamics, swirling motions in a velocity field are referred to as *vortex* [22]. From now on, the words *vortex* and *convection cell* will be used interchangeably.

Determination of vortices is an open question in the fluid dynamics literature and there is no universal method agreed upon for this task. One of the common methods is called "Vorticity Magnitude Thresholding" [23], where *vorticity* ($\boldsymbol{\omega}$) is defined as the curl of the velocity field:

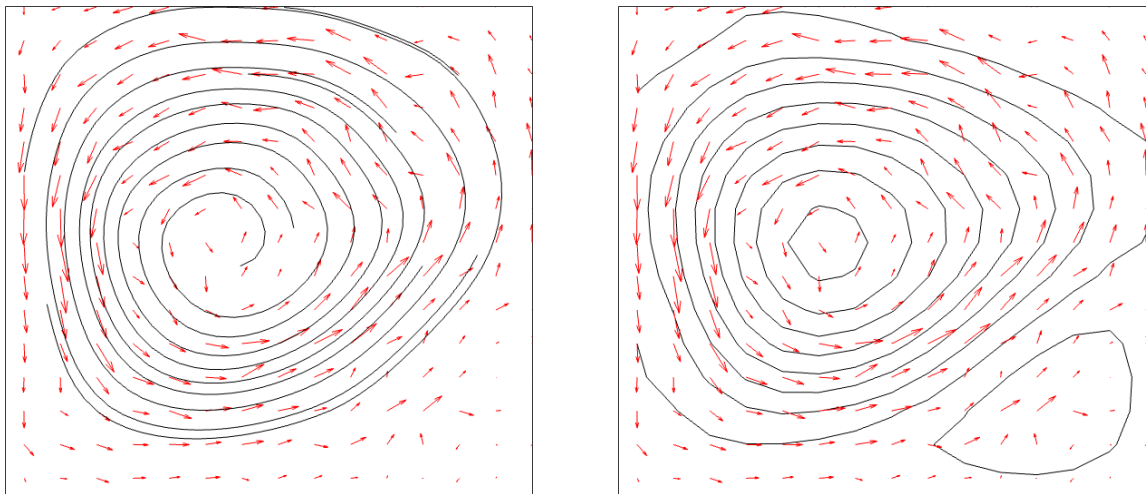
$$\boldsymbol{\omega} = \nabla \times \mathbf{v} \quad (4.10)$$

More intuitively, *vorticity* describes the local infinitesimal rotation of a given vector field. By putting a suitably chosen threshold on the magnitude of vorticity, the centre of the vortex can be identified. In 2D, the magnitude of vorticity is given by:

$$\omega = \frac{\partial v_y}{\partial x} - \frac{\partial v_x}{\partial y} \quad (4.11)$$

Due to the arbitrariness of the threshold on the magnitude the vortex centre found by this method may not always coincide with the maximum of vorticity; so this requirement is not a necessary condition for the existence of a vortex. (for example the maximum of vorticity may also appear at the edges of the flow field [22]). The approach used in this thesis is built on this method and tries to overcome the problem of thresholding.

It is assumed that the contours of the vorticity field match the streamlines (see Figure 4.5), tangential to the local velocity vectors. This assumption does not hold for every velocity field, but the velocity fields generated in our simulations turned out to satisfy it.



(a) Velocity Field and streamlines.

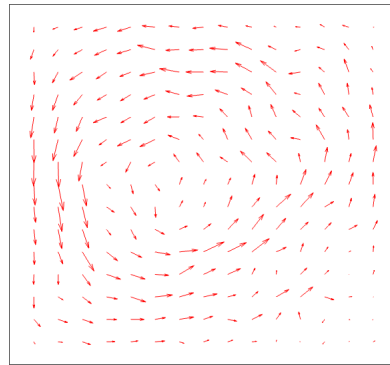
(b) Velocity field and contours of vorticity.

Figure 4.5. Streamline and vorticity contour correspondence for a given velocity field.

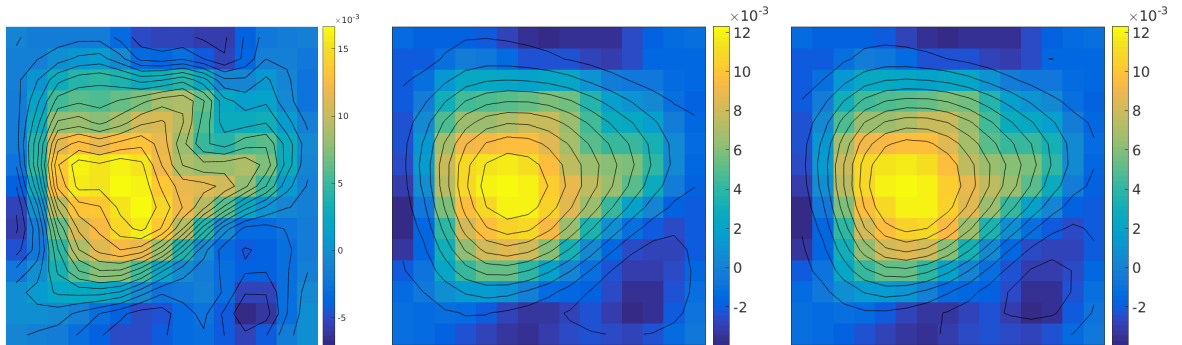
Under this assumption, the detection algorithm proceeds as follows:

- Finding the curl of the velocity field: The curl of the velocity field (see Figure 4.6(a)) over the whole domain is calculated, and the vorticity field is generated. Points of equi-vorticity are connected to obtain the vorticity contours (Figure 4.6(b)).

Due to inherent noise, it is not possible to obtain from the simulation data a perfectly smooth vorticity field, that gives perfectly elliptic contours. In order



(a) "Raw" vector field



(b) Unfiltered vorticity field (colours represent vorticity magnitude) and equi-vorticity contours (black lines)
 (c) Filtered vorticity field and equi-vorticity contours
 (d) Filtered vorticity field and modified contours

Figure 4.6. Steps of automatic detection algorithm described on a vector field obtained from a simulation with AR=0.9.

to eliminate or at least reduce the noise, the vorticity field (in Figure 4.6(b)) is smoothed using a three by three 2D Gaussian filter with standard deviation $\sigma_{filter} = 1.3$. The smoothing operation has been performed three times until the vorticity field started to reveal reasonably elliptic contours (see Figure 4.8(b)). One danger of such a filtering operation is to over-smooth the field, which can create artificial curl contours, and thus artificial vortices. Heuristically, the best results turned out to be generated by smoothing 3 times.

Contours of various sizes can be obtained by this method. The contours with smaller radii are more prone to errors as they include less data (compared to outer radii for which the centre are averaged over more data), thus they may correspond to artefacts. For this reason, contours with smaller radii are discarded (Figure 4.6(d)).

- Detecting the centres: The centre of each contour is calculated finding its centroid, i.e. as the mean of all points on the contour, in respective coordinates.
- Eliminating false centres: In order to increase the performance of the automatic detection algorithm, some assumptions have been made about the position of the vortices.

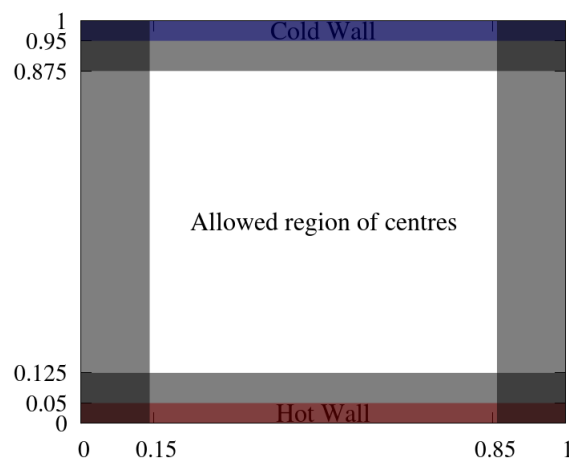


Figure 4.7. Allowed region for centres for a container with size 1×1 . Numbers on the axes represent the % distances from the boundaries.

Logically, it is not possible to have a vortex centre inside the heat layers. Thus centres detected within upper and lower heat layers are discarded as artefacts.

Second, a vortex centre is also not expected to be too close to the container boundaries, thus such centres are also discarded. The acceptable region of centres is shown on Figure 4.7.

- Clustering the centres: Ideally speaking, for a single vortex, the vorticity contours corresponding to the same convection cell should be concentric around the centre of the vortex, moreover, their centres should coincide.

In order to roughly estimate the performance of detection algorithm, an ideal vortex has been generated. This ideal vortex is given in Figure 4.8. This vortex is created by using velocity equations: $v_{x,ideal} = \Pi \sin(\Pi x) \cos(\Pi y)$ and $v_{y,ideal} = \Pi \cos(\Pi x) \sin(\Pi y)$ where $v_{x,ideal}$ and $v_{y,ideal}$ are the velocity vectors in x and y directions. The velocity field, plotted for $x \in [1,2]$ and $y \in [0,1]$ is given in Figure 4.8(a). Vorticity contours of this vortex show that the centres are concentrated on a single point 4.8(c).

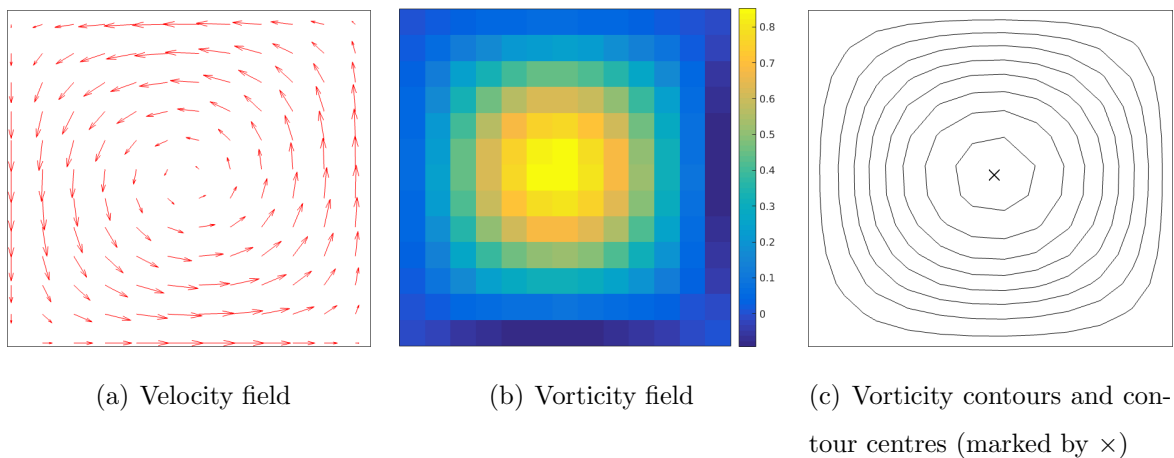


Figure 4.8. Velocity and vorticity fields of an ideal vortex.

Setting off from the case of ideal vortex, it is hoped that for the vortices presented in this thesis, which are far from being ideal but show some amount of regularity, that the centres will not strictly coincide, but will sufficiently clustered.

Thus, the contour centres are expected to be tightly packed forming well-defined clusters at the core of the vortices. Euclidean distance is used as a measure of such clustering. For two centres with i and j , this distance is defined as:

$$r_{ij} = \sqrt{(x_i - x_j)^2 + (y_i - y_j)^2}$$

Based on this measure, an Agglomerative Hierarchical Clustering algorithm has been used. This method merges the neighbouring centres that are closest to each other (in the Euclidean sense), and keeps on the merging operation until all the centres in the domain are clumped together, resulting in a distance tree, or a dendrogram (Figure 4.9).

In order to determine the number of clusters, one has to decide on where to cut this dendrogram. If the cut off the distance is too small, there will be too many clusters (leading to detection of pseudo-vortices) or conversely, if the cut off distance is too large, some of the vortices can be lost. Considering this trade-off the cut-off distance needs to be chosen heuristically for any data set.

Convection regime will consist of closed concentric curves and the clustering algorithm will classify the cores of convection cells as a single clusters. Thus, the expected number of clusters is equal to the expected number of convection cells. From the theoretical analysis, it is also known that the aspect ratio determines the number of convection cells. Based on these considerations, the following metric is proposed as an indication of the dynamic regime.

$$\zeta = \frac{\text{Number of Clusters}}{\text{Aspect Ratio}}$$

- Deciding the regime based on clusters: From the previous item, it is known that if ζ is close to unity, then the regime is convection. Put into mathematical form:

$$1 - \delta \leq \zeta \leq 1 + \delta$$

The value of δ is decided by checking the performance of the algorithm, which is then decided to be 0.4. To conclude, the regime is convection if $0.6 \leq \zeta \leq 1.4$.

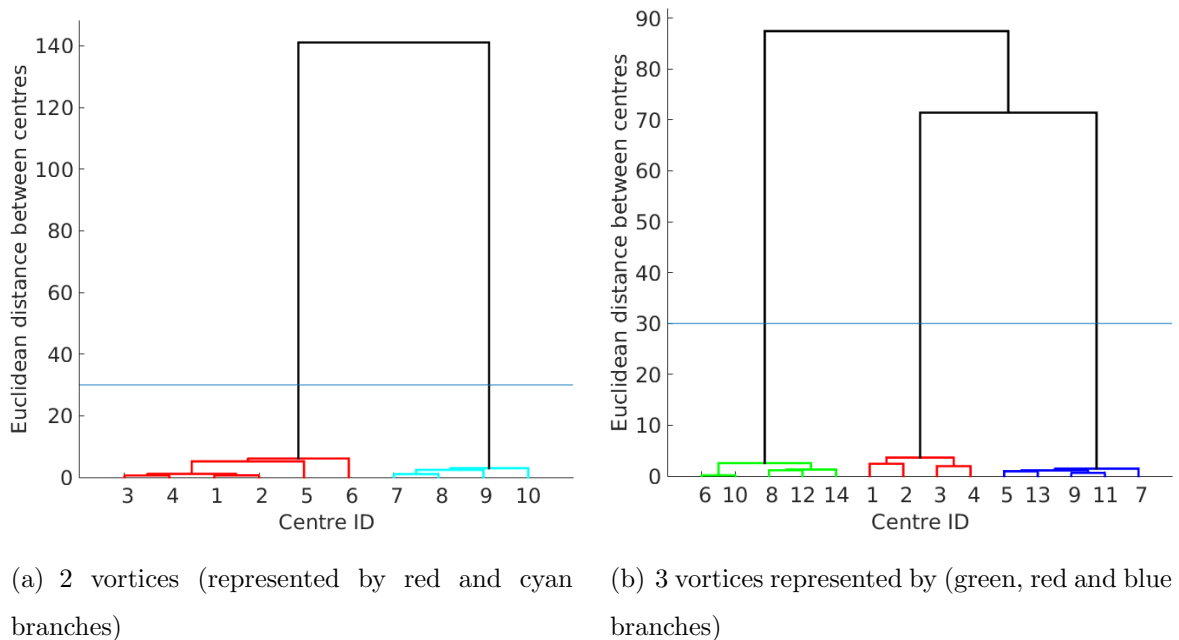


Figure 4.9. Dendrogram representing the clustering of centres, cut from Euclidean distance of 30 (vertical blue line).

4.2.2. History Analysis of a Single Particle

Convection cells considered in this thesis are self-organised structures that are generally considered as macro-scale phenomena. Therefore, it is interesting to ask whether a regime change from conduction to convection can be detected using data gathered from the whole ensemble of particles or whether the same information can also be assessed analysing the data related to a single particle.

To answer this question, two different approaches have been employed: (i) the position and velocity recordings corresponding to a randomly chosen single particle have been used to construct the velocity field and the automatic convection detection method has been applied to it, (ii) Fast Fourier Transform (FFT) analysis of the acceleration (or equivalently applied force) history has been used to spot if there exists qualitative differences between conduction and convection regimes. Here, it is assumed that the particle does not “know” its locations within the macro-scale frame, neither velocities, but can only “feel” the forces acting upon it as it interacts with the other particles around it.

4.2.2.1. Computation of the Flow Field and Automatic Detection of Convection Cells.

Velocity and position history of a randomly selected single particle has been used to construct the velocity field (as described in section 4.2.1.1) and automatic detection has been applied on this velocity field (as described in 4.2.1.2).

4.2.2.2. Automatic Detection of the Dynamic Regime from Force History.

The way to put this assumption into mathematical frame is to work with the force data of the randomly selected particle. The necessary averaging within a time window is performed via root-mean-square function of the force vector magnitude in discrete time:

$$F_{rms}(t) = \sum_{n_\tau=t-(\tau/2)}^{n_\tau=t+(\tau/2)} \sqrt{F(n_\tau)^2} \quad (4.12)$$

In order to see the periodicity of the signal, Fast Fourier Transform is applied, which is a widely used way of transforming a signal in the time domain into frequency domain. If there is a large scale periodic motion (such as the motion of a convection cell), it should be distinguished from other types of motion.

It is known that in conduction regime, the motion of particles is random, or so-called “Brownian motion”. The FFT of this type of motion is named as Brownian noise. Whereas in convection regime, the expected shape of FFT is different than Brownian noise, having certain deviations at certain frequencies.

5. SIMULATION RESULTS AND THEIR ANALYSIS

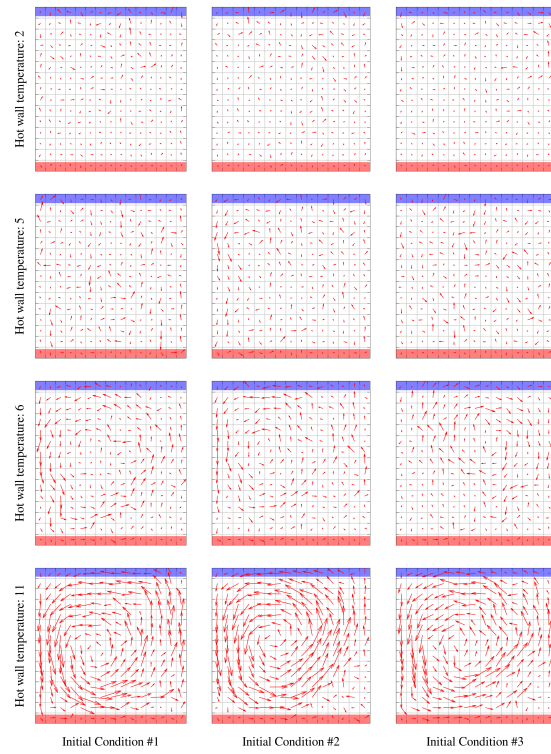
5.1. Ensemble Analysis

5.1.1. Construction of the Flow Field

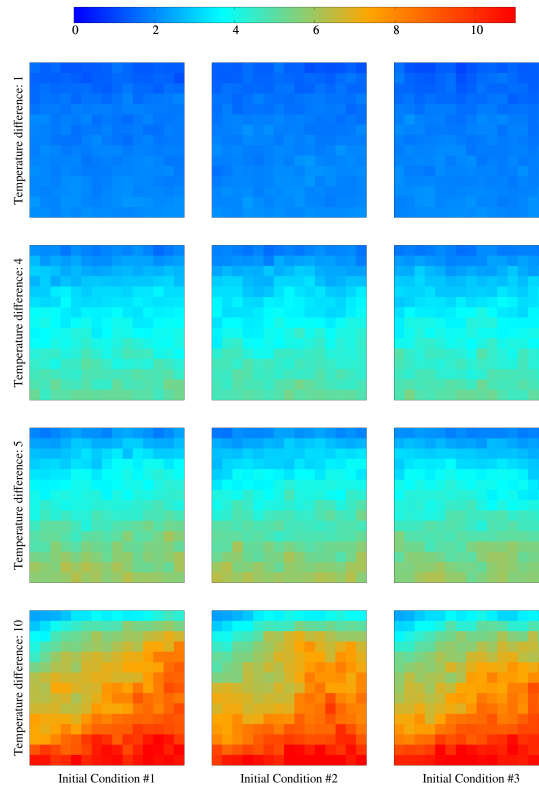
In order to determine the dependence of the dynamic regime on the temperature gradient between top and the bottom of the container (ΔT), simulations have been conducted under various ΔT s, keeping other parameters such as number density and aspect ratio of the container constant. Similarly, the dependence of the number of convection cells on the AR of the container has been investigated by repeating the same simulations with different ARs.

Figures 5.1(a), 5.2(a) and 5.3(a) represent the velocity fields and Figures 5.1(b), 5.2(b) and 5.3(b) represent the temperature fields obtained from simulations with AR=0.9, 1.4 and 1.8 respectively, using ensemble analysis method described in section 4.2.1.1. In order to show to what extent the observed phenomena depend on the initial conditions of the simulations, the same outcomes are presented for three different randomly selected initial conditions, presented in three different columns. In all figures, four rows correspond to simulations performed under four different ΔT s, in decreasing order from top to bottom.

In Figures 5.1(a), 5.2(a) and 5.3(a), from the existence of vortices within the velocity field towards higher ΔT , it can be clearly observed that the dynamic regime shifts from conduction to convection as ΔT increases. Although, it is not possible to determine the exact temperature gradient where the transition from conduction to convection occurs by looking at this data, the transition can be thought to be somewhere between $\Delta T=4$ and $\Delta T=5$. The existence of somehow hardly distinguishable weak vortices within the velocity field of $\Delta T=5$ and inexistence of such structures within the velocity field of $\Delta T=4$ supports this observation. The transition temperature gradient seems to be independent of AR and initial conditions and the same for the different

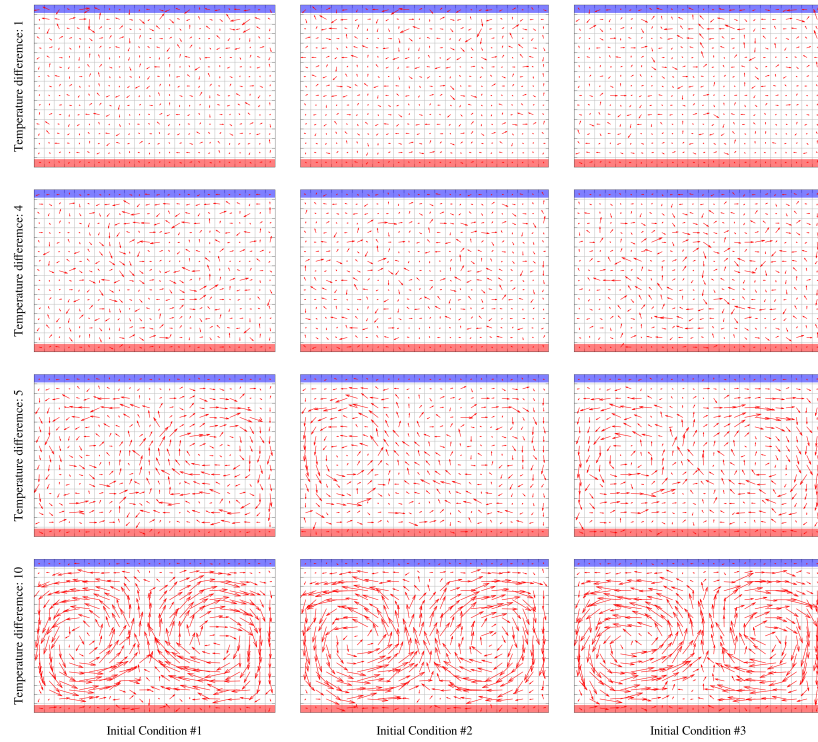


(a) Velocity Field

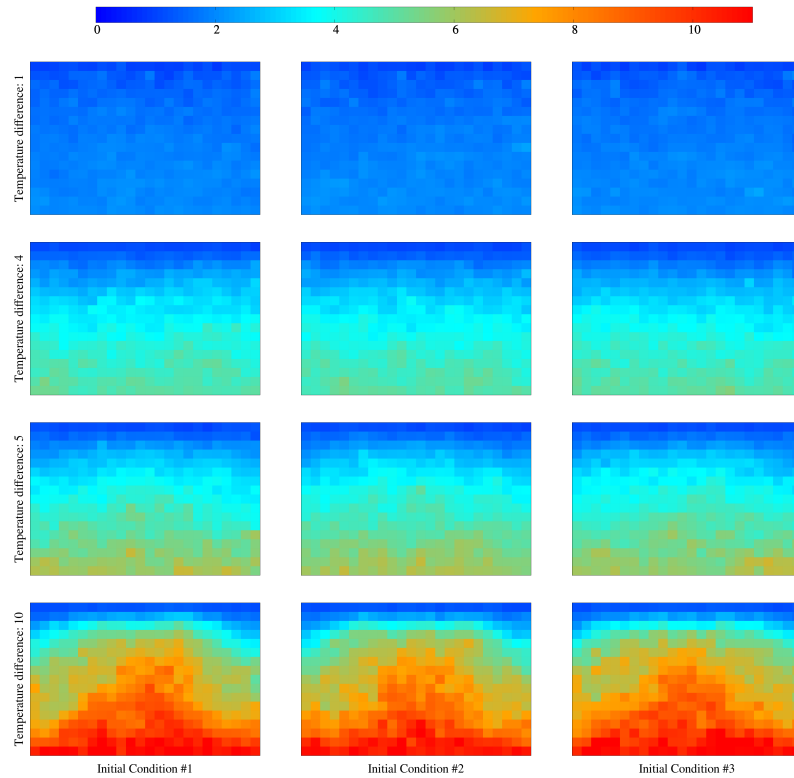


(b) Temperature Field

Figure 5.1. Flow Field for AR=0.9.

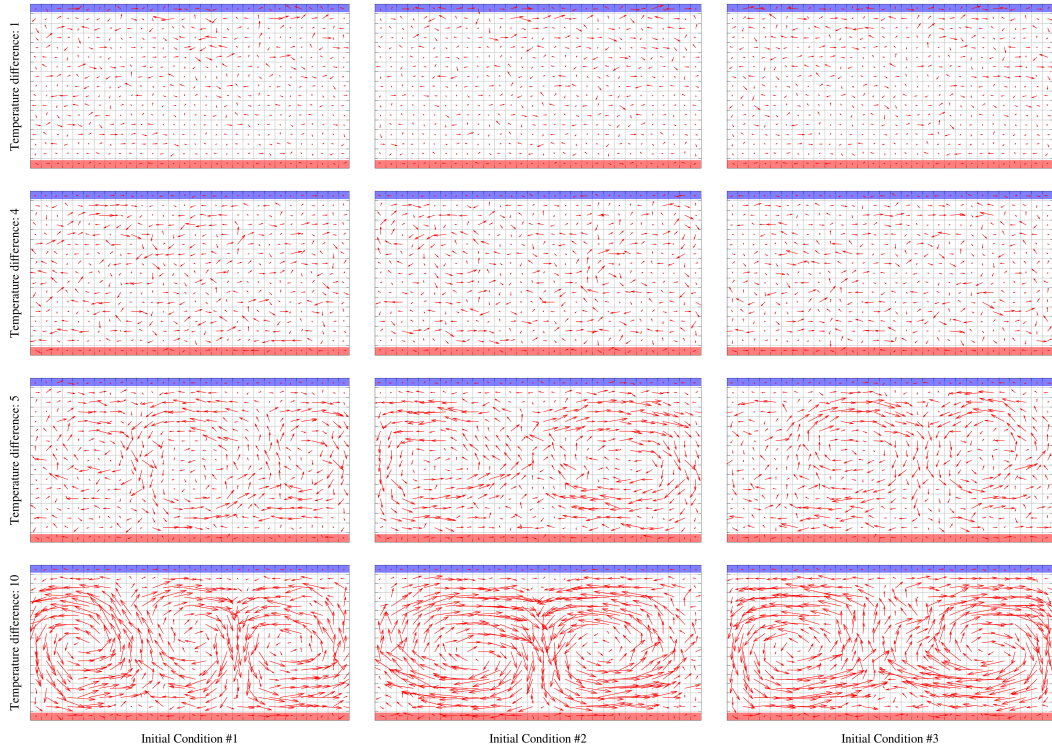


(a) Velocity Field

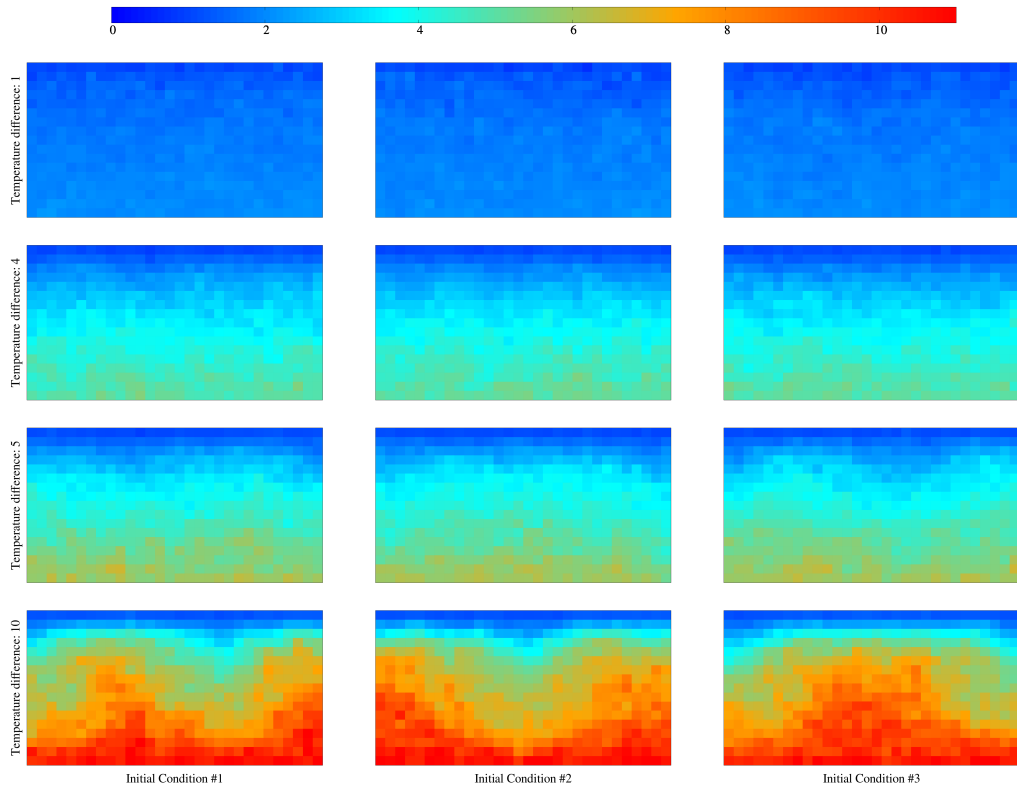


(b) Temperature Field

Figure 5.2. Flow Field for AR=1.4.



(a) Velocity Field



(b) Temperature Field

Figure 5.3. Flow Field for AR=1.8.

systems with identical number densities.

In accordance with empirical results reported in the literature, as AR increases, number of vortices increases and number of possible dynamic regimes also increases.

The last rows of Figures 5.1(a), 5.2(a) and 5.3(a) illustrate the different types of dynamic regimes observed at convection. For AR=0.9 (Figure 5.1), all three initial conditions give rise to single counter clockwise rotating convection cells. For AR=1.4 (Figure 5.2), all three initial conditions give rise to double oppositely rotating convection cells. In the case of AR=1.8 (Figure 5.3, three different types of structures are observed for three different initial conditions: a case with 3 vortices (Initial Condition #1) and two cases with two vortices (Initial Conditions #2 and #3). The case of two vortices show different characteristics: in former, the motion in the middle of the two vortices is downwards (Initial Condition #2), however, in the latter the motion in the middle of the two vortices is upwards (Initial Condition #3). These observations suggest that the initial conditions affect the number and the sense of rotation of the convection cells.

The onset of convection creates a characteristic change also in the temperature fields (Figures 5.1(b), 5.2(b) and 5.3(b)). In the conduction regime, lower ΔT , the temperature gradient seems to be in vertical direction only (first two rows of Figures 5.1(b), 5.2(b) and 5.3(b)). In convection regime, however, the gradients become diagonal (last rows of Figures 5.1(b), 5.2(b) and 5.3(b)). It is even possible to guess the number and sense of rotation of the convection cells from these fields. For example, in the last row of Figure 5.1(b), temperature gradient seems to be in the direction of left upper corner of the container. Looking at the corresponding velocity field at Figure 5.1(a), it can be seen that this direction indicates a counter clockwise rotating convection cell.

5.1.2. Automatic Detection of Convection Cells

As a demonstration of the performance of the automatic detection algorithm, it has been applied on several velocity fields. For the example demonstrated on Figure 5.4, vector field from the simulation with $AR=0.9$, initial condition #3 has been used.

As seen in the last step in Figure 5.4(d), two vortex centres are detected within the field, which is visually wrong. In order to discard the false vortex centres, the methods described in section 4.2.1.2 are applied. After the elimination, Figure 5.5 is obtained.

Similarly, for the case of two and three vortices algorithm is applied on vector fields with $AR=1.8$ with initial conditions #1 and #3 (Figure 5.3(a)). Automatically detected vortex centres and their clusters are given in Figures 5.6 and 5.7.

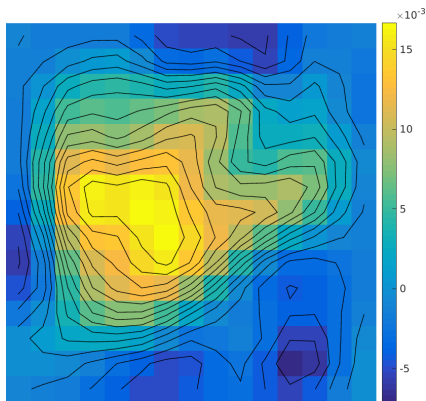
The automatic detection algorithm has produced satisfactory results, predicting the dynamic regime and also number of clusters correctly. Nevertheless, as the aspect ratio increases the performance of the automatic convection detection algorithm deteriorates.

5.2. History Analysis of a Single Particle

5.2.1. Construction of the Flow Field

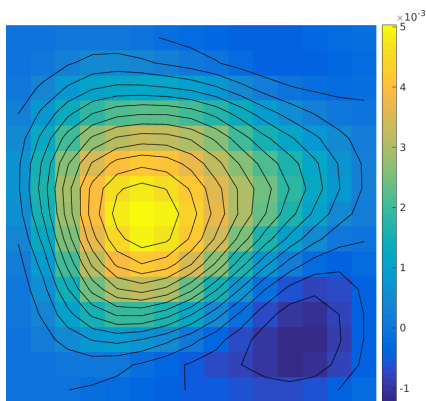
Using position and velocity history of a randomly selected particle from diverse simulations, trajectories of that particle within the container and velocity field using coarse graining is constructed.

For a particle randomly selected from simulation with $AR=0.9$ and initial condition #1, trajectories and velocity fields for $\Delta T = 10$ and $\Delta T = 4$ obtained at the end of different time steps are given in Figures 5.8 and 5.9.



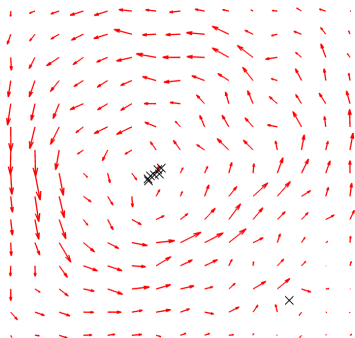
(a) Obtaining the equi-vorticity contours

Curl of the velocity field is computed and a new field, vorticity field is constructed as shown on the left. The points of equal vorticity are connected and black contours are obtained.



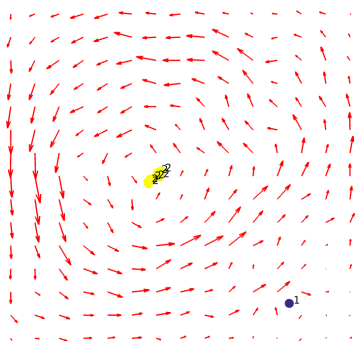
(b) Smoothing the contours

The vorticity field is smoothed using a Gaussian image filter, then the contours are replotted. As seen, these contours are much smoother and look more like ellipses/circles.



(c) Finding the contour centroids

Centroids of the contours are calculated and plotted on the original vector field. These centroids represent the centres of the rotational flows within the velocity field.



(d) Finding the centre of the convection cell

In order to find the centre of the convection cell the contour centroids are clustered.

Figure 5.4. Steps performed in the automatic detection of a single convection cell.

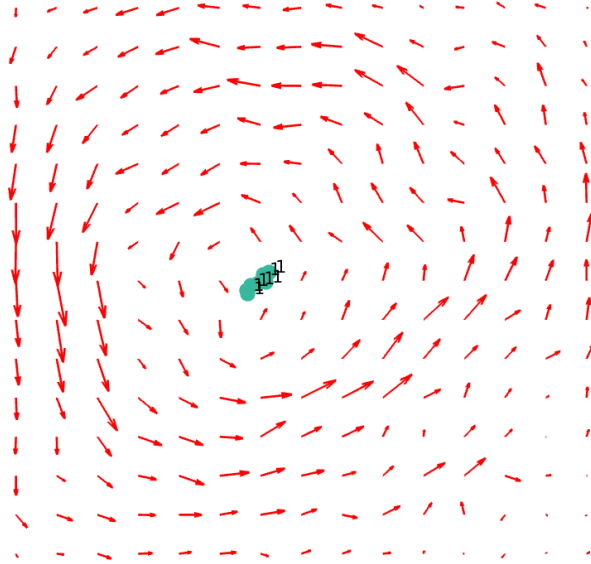


Figure 5.5. Location of the centre of single convection cell.

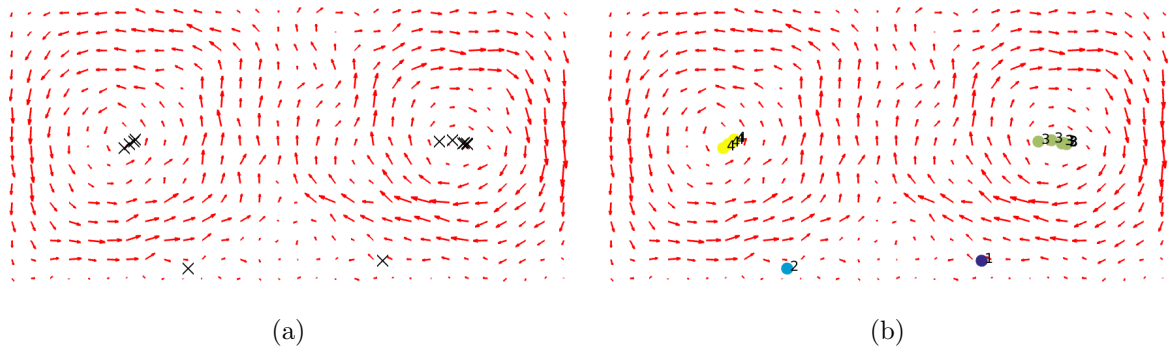


Figure 5.6. (a) Centroids and (b) their clustering for a velocity field with 2 convection cells.

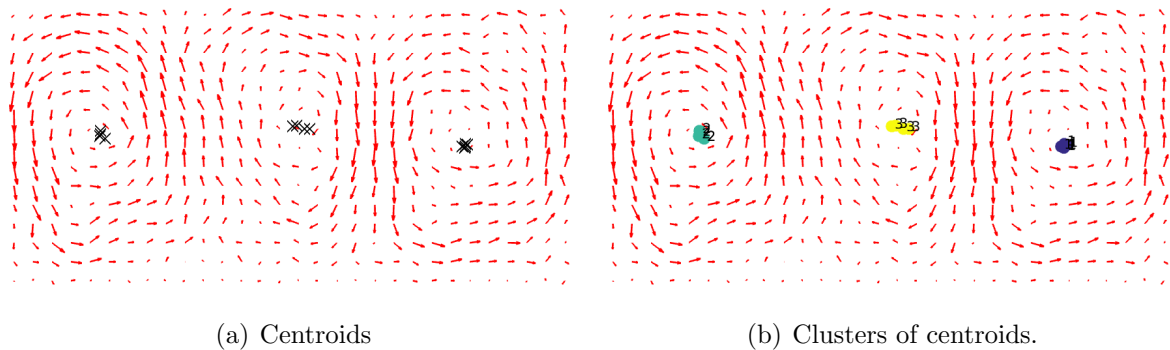


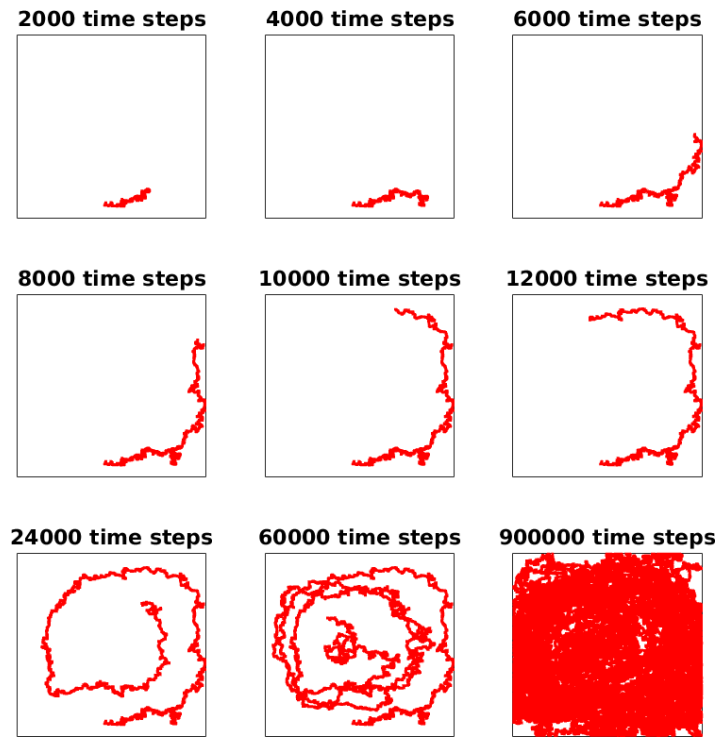
Figure 5.7. (a) Centroids and (b) their clustering for a velocity field with 3 convection cells.

In Figure 5.8(a), the particle is observed to move in circles as time proceeds and constructs the shape of the convection cell. The sense of rotation of the cell matches well the sense of rotation of the vortex obtained through ensemble analysis (Figure 5.1(a)). The velocity field seen on Figure 5.8(b), is equivalent with that of 5.1(a). Thus, it can be said that the analysis of the history of a single particle provides an information equivalent to what can be obtained from ensemble analysis provided that a long enough history is considered.

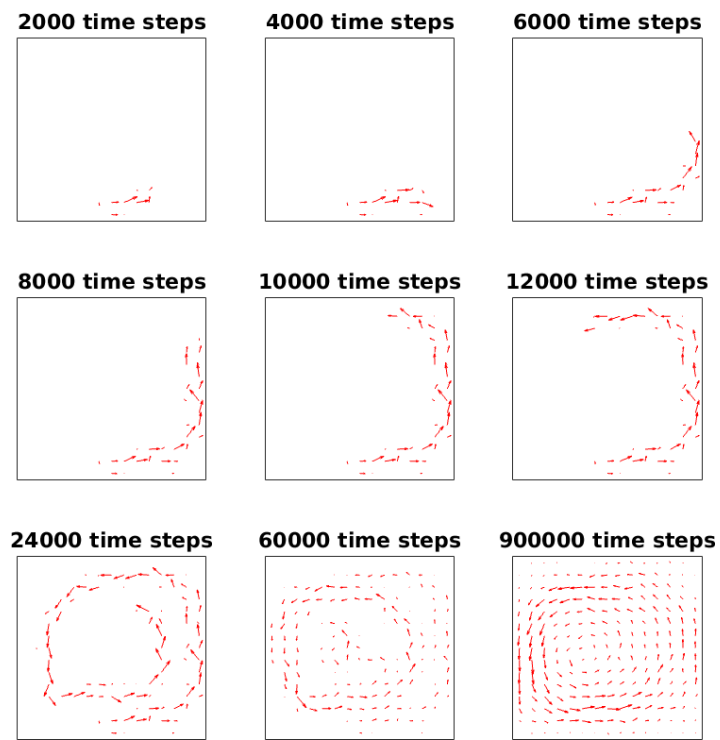
However, in the case of conduction ($\Delta T = 4$), this claim cannot be made. First of all, a particle in conduction regime does not sufficiently visit all regions of the container (Figure 5.9(a)). Also, the velocity field seen in Figure 5.9(b) is not equivalent to the one seen on Figure 5.1(a). Thus, it can be said that, ensemble analysis and history analysis of a single particle do not provide the same information in the conduction regime.

5.2.2. Automatic Detection of Convection Cells

Automatic detection algorithm has been applied to velocity fields constructed using the velocity history data of randomly selected particles. To demonstrate how the performance of the algorithm depends on the randomly chosen particle, results have been presented for one particle in conduction regime and for three different particles

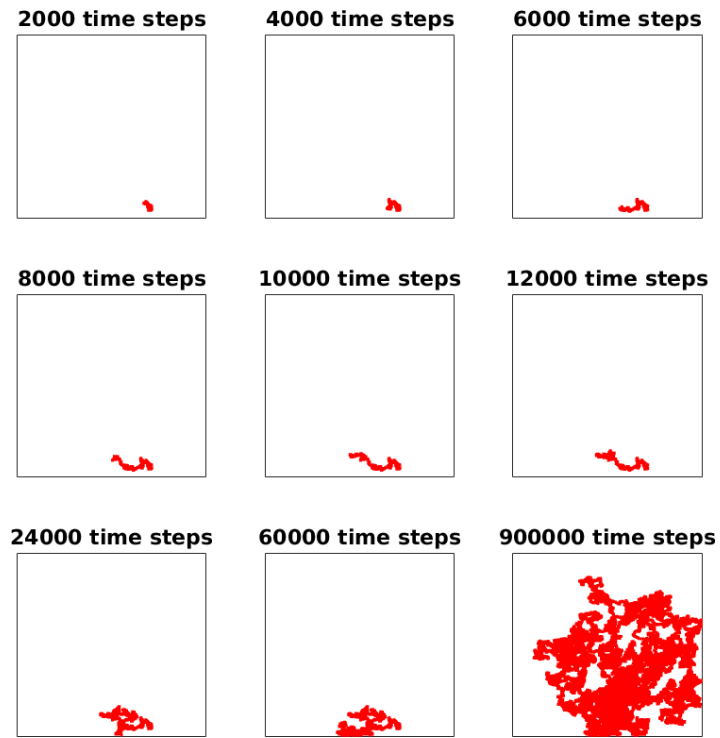


(a) Trajectory within the container

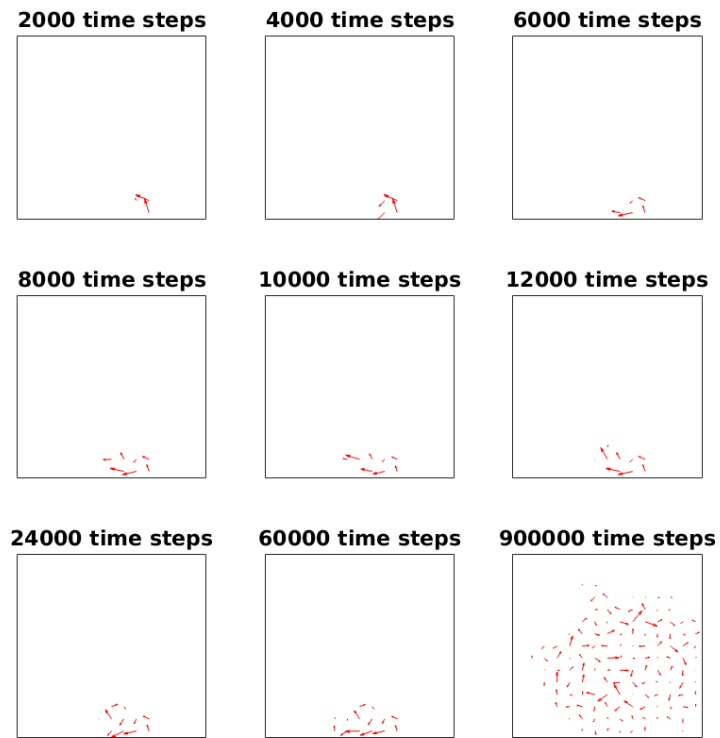


(b) Velocity Field

Figure 5.8. Velocity and position history of a single particle at convection regime ($\Delta T = 10$).



(a) Trajectory within the container



(b) Velocity Field

Figure 5.9. Velocity and position history of a single particle at convection regime ($\Delta T = 4$).

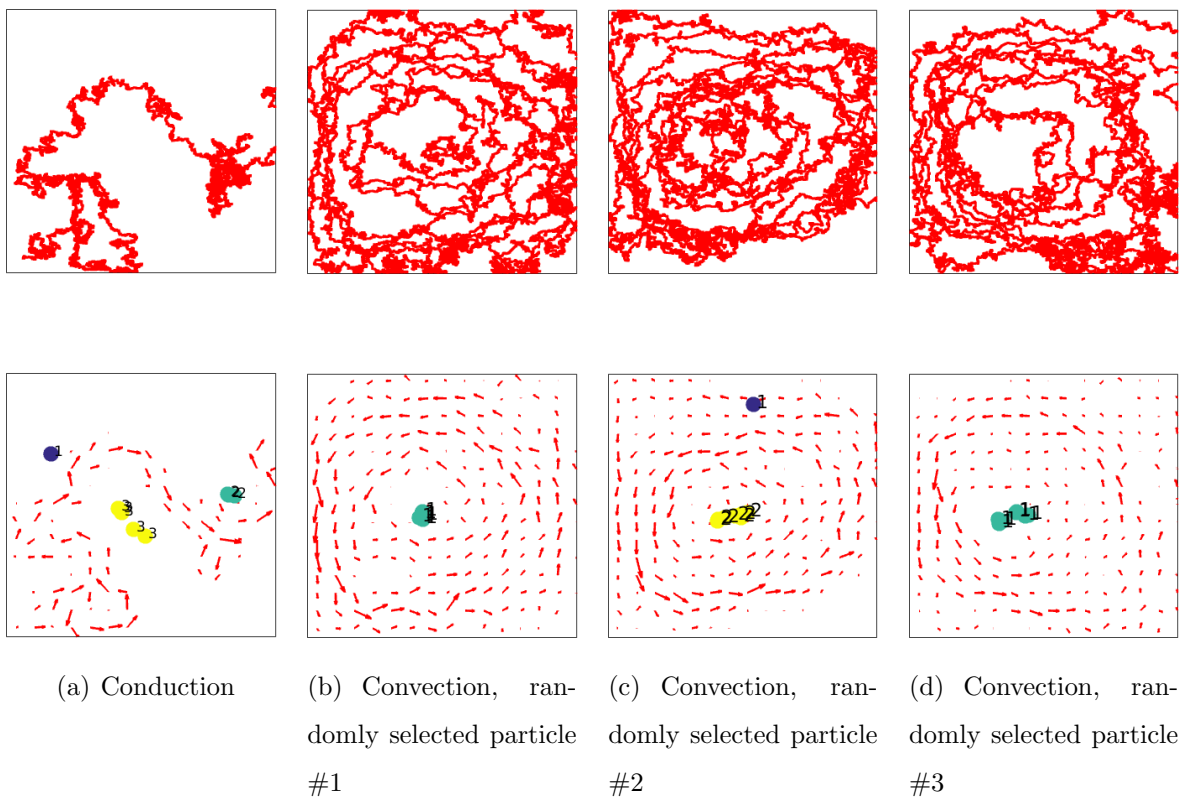


Figure 5.10. Automatic detection algorithm applied on single particle history, case of single vortex.

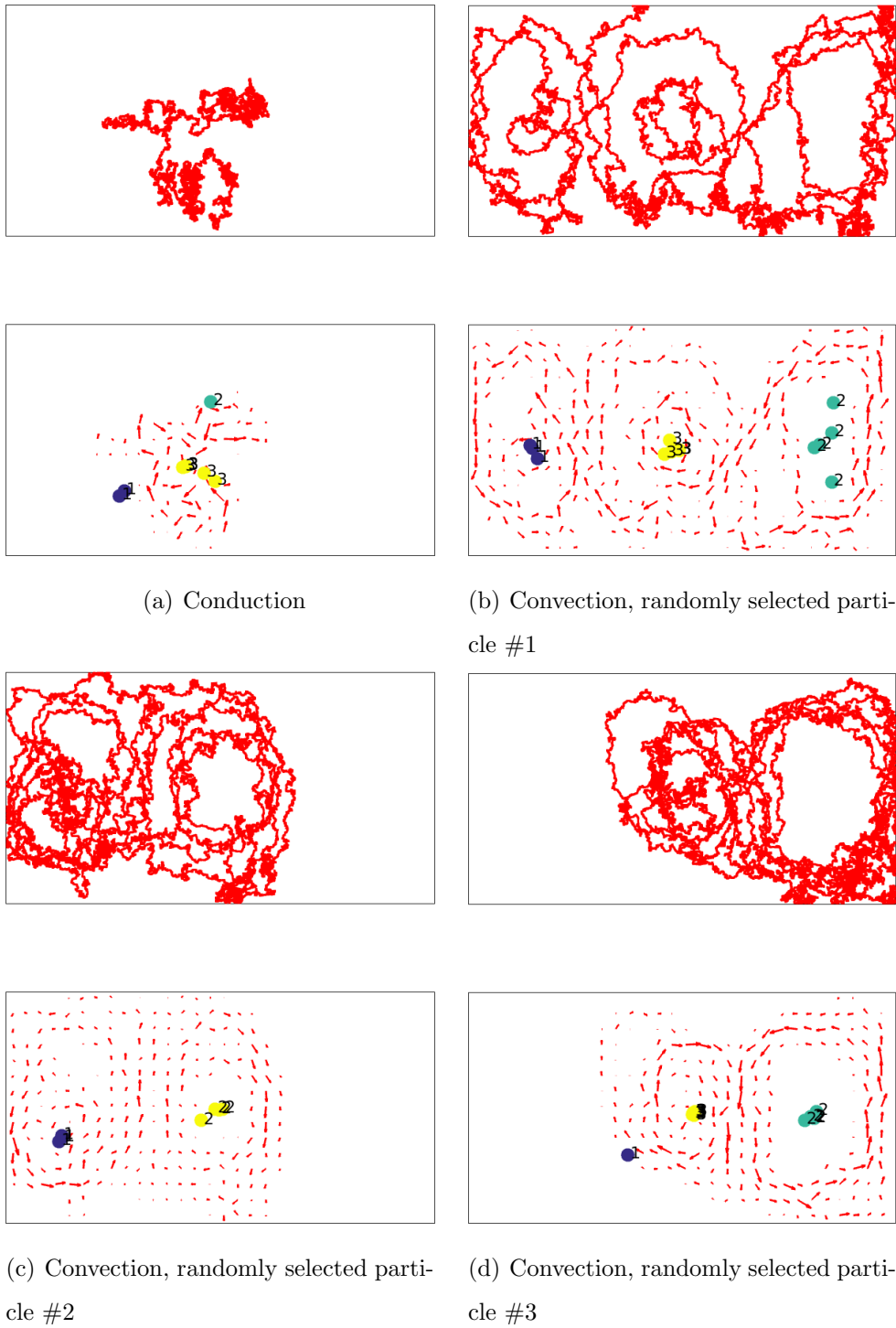


Figure 5.11. Automatic detection algorithm applied on single particle history, case of three vortices.

selected from the same simulation in the convection regime (Figures 5.10 and 5.11).

The results of the algorithm for the simulation with a single vortex is given in Figure 5.10. The number of vortices and the regime is rather correctly predicted. However in the conduction regime, the algorithm has produced faulty results since the velocity field could not be generated for a subregion of the container.

For the case with three vortices, other problems have occurred. Seen in Figure 5.11, there are cases where the particle does not visit all three convection cells (Figures 5.11(c),5.11(d)). This case, again, poses problems to the detection algorithm, which requires the full velocity field information within the container. In those cases, fewer vortices than the actual number are detected. But if the particle chosen happens to visit all vortices, the algorithm can detect the correct number of vortices (Figure 5.11(b)).

It seems that additional conditions and corrections need to be developed such that the detection algorithm can be used in simulations with higher ARs.

5.2.3. Can the Macro-Scale Dynamic Regime be Detected from the Particle Perspective ?

It has been shown that, in conduction and convection regimes, there are qualitative differences at position trajectories and velocity fields of a single particle constructed from history of positions and velocities (Figures 5.9 and 5.9). However, the question of a particle having “access” to these variables for identifying its regime is a matter of debate. For this reason, as described in section 4.2.2.2, it is assumed that the particle has only access to its force history. This assumption seems reasonable, as forces are the relative effects of the neighbouring particles upon the particle in consideration, rather than position and velocity which requires information from a global coordinate system.

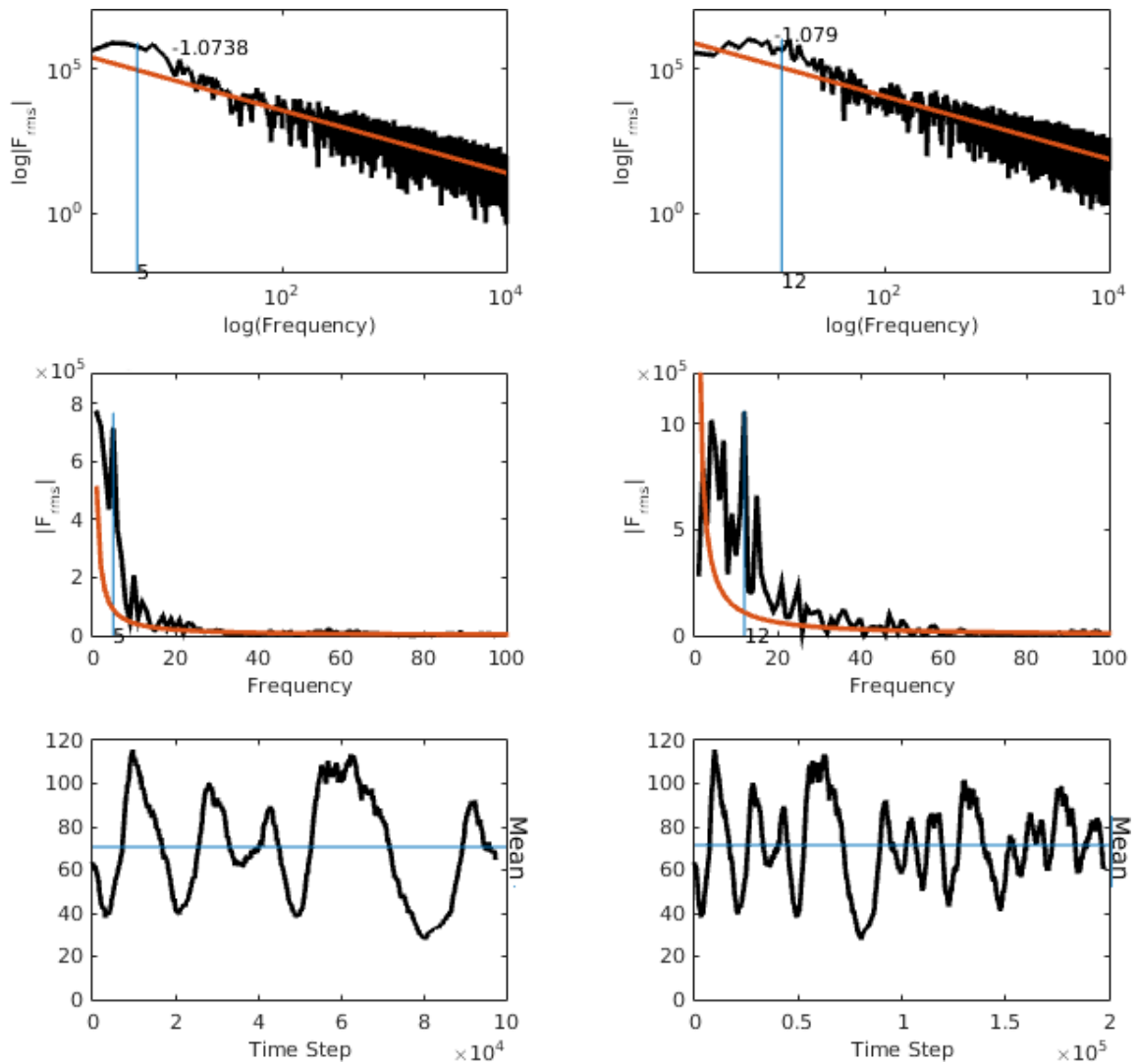
Figure 5.12 shows the force history of a randomly selected particle in convection regime, when $\Delta T = 10$. In the last rows of this figure, root-mean-squared value of force

history, F_{rms} is plotted versus time steps. Root-mean-square operation is performed as explained in section 4.2.2.2 with a time window of 2500 time steps. The value of this window is chosen to be approximately one eighth of the period of rotation of a single particle. This period, which turned out to be approximately 20000 time steps, is decided by following a single particle as it proceeded its trajectory in convection regime (see Figure 5.8(b)).

First two rows of Figure 5.12 are respectively the FFT of F_{rms} plotted versus frequency, in logarithmic and linear scales. For ease of readability, first 100 frequency components are given for linear plots.

Figure 5.13 is similarly organised, where columns represent randomly selected particles at conduction regime under $\Delta T = 1$, $\Delta T = 4$ and $\Delta T = 5$. Log-log plot of FFT of these graphs seem to fit well to a line with slope -1 (red line). This is the sign of “Brownian motion”, which represents randomness. The same curve fit is also applied for linear FFT, which seems to agree well with data again. However, it should be noted that as ΔT increases, deviations from Brownian line at low frequencies occurs. Randomness of the force history can also be observed on row 3 of this figure, history of F_{rms} is plotted. There appears no clear regularity in time history of F_{rms} .

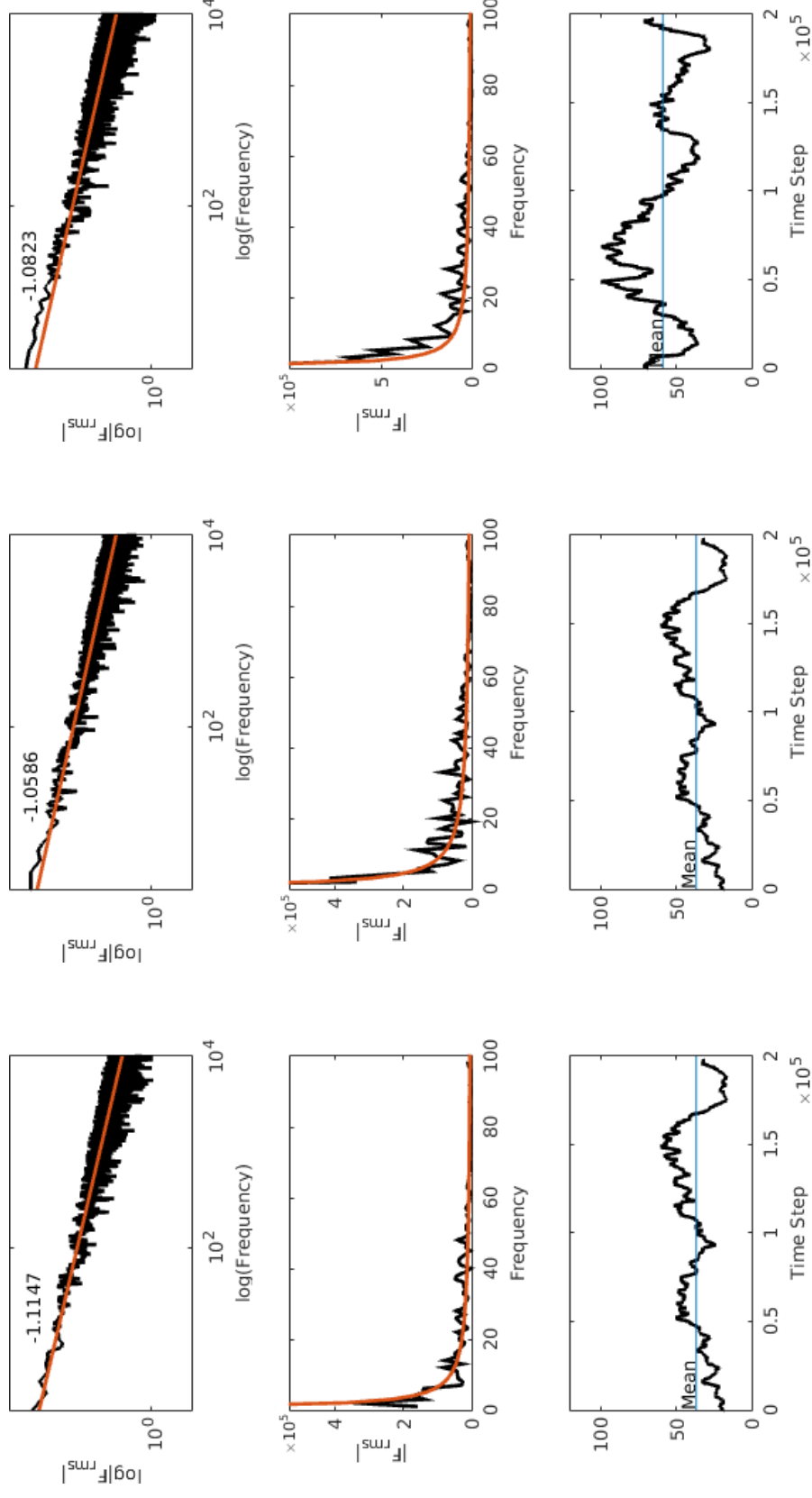
When it comes to force history obtained from a particle in convection, almost regular oscillations of F_{rms} values are observed, which is a sign of convective rotating motion. This sign is also clear on FFT plots, which deviate considerably from Brownian line at low frequencies. The maximum deviation from this line is marked with blue horizontal lines on first two rows of Figure 5.12. The points that these lines intersect the frequency axis match well with the number of rotations that the particle performs. For example, in Figure 5.12(a), F_{rms} graph shows approximately 5 rotations and the intercept of blue line with frequency axis is also 5.



(a) (Top) Logarithm of the FFT of rms value of force (Middle) FFT of rms value of force (Bottom) Rms value of force acting on particle at convection regime during 100000 time steps

(b) (Top) Logarithm of the FFT of rms value of force (Middle) FFT of rms value of force (Bottom) Rms value of force acting on particle at convection regime during 200000 time steps

Figure 5.12. Force history and its FFT for a particle in convection regime.



(a) (Top) Log of the FFT of rms value of force (Middle) FFT of rms value of force (Bottom) Rms value of force acting on particle at $\Delta T = 1$ during 200000 time steps

(b) (Top) Log of the FFT of rms value of force (Middle) FFT of rms value of force (Bottom) Rms value of force acting on particle at $\Delta T = 4$ during 200000 time steps

(c) (Top) Log of the FFT of rms value of force (Middle) FFT of rms value of force (Bottom) Rms value of force acting on particle at $\Delta T = 5$ during 200000 time steps

Figure 5.13. Force history and its FFT for a particle in conduction regime under three different temperature gradients.

6. CONCLUSION

The main purpose of this thesis was to understand the process of self-organisation in Bénard experiment using molecular dynamics. Simulations have revealed that this macro-scale phenomenon is indeed observable in the micro-scale model.

Simulation results show that the model variables of micro-scale simulation, namely particle interactions, velocities, number density etc. could be chosen so that qualitative analogies could be drawn between micro-scale and macro-scale models based on the dynamic regime. It has been observed that, for a given number density, boundary conditions, initial conditions and AR, it is the temperature gradient that determines the dynamic regime, and that the transition temperature from conduction to convection is independent of these parameters. Moreover, for given number density, boundary conditions and temperature gradient, the number of vortices in convection regime depends solely on the aspect ratio and the initial conditions. As the aspect ratio increased, the number of vortices increased. Initial conditions also have an effect on number of vortices, but more importantly, they effect the rotation sense of vortices.

It has been shown that the curl of the velocity field can be used to discriminate whether the system is in the conduction or convection regime. The automatic detection algorithm developed in this thesis has been found to perform well for data extracted from an ensemble for low AR. However, the algorithm was found to be unemployable for velocity history data obtained from a single particle at conduction. As AR increased, dynamic behaviour became richer, so this algorithm was found to be shortcoming for those cases as well.

Furthermore, a theoretically interesting and original question has been posed whether the emergence of macro-scale organisation is assessable from the micro-scale perspective of a particle, which is assumed to have no information about its position and velocity in global coordinates. This question can be particularly meaningful in multi-agent systems where the agents have some level of cognitive capacity. Frequency

analysis of the fluctuations in the rms value of the total force acting on a particle has been found to provide enough clue to distinguish conduction and convection regimes, provided that the considered force history is long enough, i.e. longer than some reasonable multiple of a convection period. Based on this observation, it was concluded that if a particle has access to its force data, it would be aware of the regime that it is in.

REFERENCES

1. Manneville, P., *Dynamics of Spatio-Temporal Cellular Structures: Henri Bénard Centenary Review*, pp. 41–65, Springer New York, 2006.
2. Rapaport, D. C., *The Art of Molecular Dynamics Simulation*, Cambridge University Press, 2004.
3. Flake, G. W., *The Computational Beauty of Nature: Computer Explorations of Fractals, Chaos, Complex Systems, and Adaptation*, MIT Press, 1998.
4. Haken, H. and J. Portugali, “Information and Self-Organization”, *Entropy*, Vol. 19, No. 1, 2017.
5. Camazine, S., *Self-organization in Biological Systems*, Princeton University Press, 2003.
6. Prokopenko, M., “Guided Self-Organization”, *HFSP Journal*, Vol. 3, No. 5, pp. 287–289, 2009.
7. Rayleigh, L., “On Convection Currents in a Horizontal Layer of Fluid, When the Higher Temperature is on the Under Side”, *The London, Edinburgh, and Dublin Philosophical Magazine and Journal of Science*, Vol. 32, No. 192, pp. 529–546, 1916.
8. Perkins, A. C., *Mechanisms of Instability in Rayleigh-Bénard Convection*, Ph.D. Thesis, Georgia Institute of Technology, 2011.
9. Allen, M. P. and D. J. Tildesley, *Computer Simulation of Liquids*, Oxford University Press, 1989.
10. Rapaport, D., “Molecular-dynamics Study of Rayleigh-Bénard Convection”, *Phys-*

- ical Review Letters*, Vol. 60, No. 24, 1988.
11. Kundu, P. and L. Cohen, *Fluid Mechanics*, Academic Press, 1990.
 12. Mareschal, M. and E. Kestemont, “Experimental Evidence for Convective Rolls in Finite Two-Dimensional Molecular Models”, *Nature*, Vol. 329, No. 6138, 1987.
 13. Rapaport, D., “Unpredictable Convection in a Small Box: Molecular Dynamics Experiments”, *Physical Review A*, Vol. 46, No. 4, 1992.
 14. Rapaport, D., “Hexagonal Convection Patterns in Atomistically Simulated Fluids”, *Physical Review E*, Vol. 73, No. 2, 2006.
 15. Mugnai, M. L., S. Caprara, G. Ciccotti, C. Pierleoni and M. Mareschal, “Transient Hydrodynamical Behavior by Dynamical Nonequilibrium Molecular Dynamics: The Formation of Convective Cells”, *The Journal of Chemical Physics*, Vol. 131, No. 6, 2009.
 16. Rapaport, D., “Time-dependent Patterns in Atomistically Simulated Convection”, *Physical Review A*, Vol. 43, No. 12, 1991.
 17. Puhl, A., M. M. Mansour and M. Mareschal, “Quantitative comparison of Molecular Dynamics with Hydrodynamics in Rayleigh-Bénard Convection”, *Physical Review A*, Vol. 40, 1989.
 18. Hartkamp, R. M., *A Molecular Dynamics Study of Non-Newtonian Flows of Simple Fluids in Confined and Unconfined Geometries*, Ph.D. Thesis, University of Twente, 2013.
 19. Karniadakis, G. E., A. Beskok and N. Aluru, *Microflows and Nanoflows: Fundamentals and Simulation*, Vol. 29, Springer Science & Business Media, 2006.
 20. Cengel, Y. A. and J. M. Cimbala, *Fluid Dynamics: Fundamentals and Applications*, McGraw Hill, New York, 2006.

21. Plimpton, S., “Fast Parallel Algorithms for Short-Range molecular dynamics”, *Journal of computational physics*, Vol. 117, No. 1, pp. 1–19, 1995.
22. Berdahl, C. and D. Thompson, “Eduction of Swirling Structure Using the Velocity Gradient Tensor”, *AIAA journal*, Vol. 31, No. 1, pp. 97–103, 1993.
23. Holmén, V., *Methods for Vortex Identification*, Master’s Thesis, Lund University, 2012.

APPENDIX A: NUMERICAL INTEGRATION ALGORITHM

Equations of motion are solved numerically using integration algorithms that are based on finite difference methods.

All algorithms used in molecular dynamics are based on truncated Taylor series:

$$x(t + \Delta t) = \sum_{n=0}^{\infty} \frac{d^{(n)}x}{dt^{(n)}} \frac{\Delta t^n}{n!} = x(t) + \dot{x}(t) \Delta t + \ddot{x}(t) \frac{(\Delta t)^2}{2} + H.O.T. \quad (\text{A.1})$$

where Δt is the time step and H.O.T. represent the higher order terms.

In the literature, there exist many different numerical algorithms used for molecular dynamics simulation. With regard to molecular dynamics there are two widely used methods [2] namely the leapfrog-type method and predictor-corrector method.

Velocity-Verlet is a widely used low order (second order) integration method that is known to have good conservation properties. For these reasons, this algorithm has been implemented in this thesis. The position and velocity integration of Velocity-Verlet are given by the following equations:

$$\begin{aligned} x(t + \Delta t) &= x(t) + \underbrace{\dot{x}(t)}_{v(t)} \Delta t + \underbrace{\ddot{x}(t)}_{F(t)/m} \frac{(\Delta t)^2}{2} \\ v(t + \Delta t) &= v(t) + \frac{1}{2} \Delta t \left(\underbrace{\dot{v}(t)}_{F(t)/m} + \underbrace{\dot{v}(t + \Delta t)}_{F(t+\Delta t)/m} \right) \end{aligned} \quad (\text{A.2})$$

The terms on the right hand side of equations A.2 are either given initially / known from the previous time step (such as $x(t)$ and $\dot{x}(t)$) or computed from the simulation ($\ddot{x}(t)$, $\dot{v}(t)$, $\dot{v}(t + \Delta t)$).

Choice of time step, Δt is a matter of compromise. Large Δt allows fast computation of simulation results corresponding to the system's behaviour for a given real-time interval. The price for it is, however, large integration errors. Conversely, these errors can be reduced by choosing small Δt at cost of long simulation runs.